River discharge and bathymetry estimations from SWOT altimetry measurements

Kévin Larnier, Jerome Monnier, P.-A. Garambois, J. Verley

River discharge and bathymetry estimations from SWOT altimetry measurements

K. Larnier(1)(2)(3)(4), J. Monnier(2)(3)*, P.-A. Garambois(4)(5), J. Verley (2)(3)(4)

(1) CS corporation, Business Unit Espace, Toulouse, France.
(2) Institut de Mathématiques de Toulouse (IMT), France.
(3) INSA Toulouse, France.
(4) ICUBE, Strasbourg, France.
(5) INSA Strasbourg, France.
* Corresponding author: jerome.monnier@insa-toulouse.fr
Keywords. Discharge, bathymetry, inference, data assimilation, altimetry, SWOT, ungauged rivers.

Abstract

An inversion algorithm to estimate the discharge of rivers observed by the forthcoming SWOT mission (wide swath altimetry) is developed and assessed in detail. The algorithm relies on an advanced variational data assimilation formulation applied to the Saint-Venant equations (1D shallow-water) combined with a lower complexity model (low Froude assumption and locally stationary). This modeling approach enables to estimate from the altimetry measurements the three flow features: the discharge $Q(t)$ associated with an effective bathymetry $b(x)$ and a (non constant) roughness coefficient K. The river geometry is built up with effective cross sections defined from the altimetry measurements. The numerical results are analyzed for three rivers ($\sim$ 100 km long each) presenting rapid flow variations compared to the observation frequency. Two scenarios of observation are considered: frequent satellite overpasses corresponding to the SWOT Cal-Val orbit ($\sim$1 day period) and SWOT like data corresponding to a $\sim$21 days period with 1 to 4 passes at mid-latitudes. Given prior mean values (of Q or/and b), the numerical experiments demonstrate that the inference of the river discharge $Q(t)$ and the bathymetry profile $b(x)$ may be accurate. Various prior values sources are investigated in view of worldwide applications. Once the assimilation of a long period of measurements is done (e.g. one year long time series), the low complexity flow model is correctly calibrated and provides accurate discharge estimations in real-time from newly acquired measurements.

1 Introduction

While in-situ observability of the continental water cycle and river flows is declining, a myriad of satellites for earth observations provide increasingly accurate measurements. The future Surface Water and Ocean Topography (SWOT) mission (CNES-NASA, planned to be launched in 2021) equipped with a swath mapping radar interferometer will provide river surfaces mapping at a global scale with an unprecedented spatial and temporal resolution on Water Surface (WS) height, width and slope - decimetric accuracy on WS height averaged over 1 km^2 (Rodríguez, 2012). SWOT will cover a great majority of the globe with relatively frequent revisits (1 to 4 revisits per 21 days repeat cycle). By complementing decades of nadir altimetry in inland waters (Calmant et al., 2016), SWOT should offer the opportunity to increase our knowledge of the spatial and temporal distribution of hydrological fluxes see e.g. Biancamaria et al., 2010, 2016.

Thanks to this increased observability of WS worldwide, it will be possible to address a variety of inverse problems in surface hydrology and related fields (see e.g. Ottle and Mahfouf, 2016). Given these WS measurements (elevation, water mask extents), the challenging inverse problem involves infering the discharge, the unobservable cross sections, the friction parametrization and any lateral contributions. The estimation of the discharge is more or less challenging depending on the space-time WS observation density, the prior information quality and the measurement errors. Recent literature addresses some of these inverse questions in a purely remote sensing context (see e.g. Biancamaria et al., 2016 for a review). Several low-complexity methods have been developed; they are based either on steady-state flow models like the Manning-Strickler's law or empirical hydraulic geometries power-laws (Bjerklie, 2007; Durand et al., 2014; Garambois and Monnier, 2015; Yoon et al., 2016). In Durand et al., 2016, numerous approaches are compared on 19 rivers with artificially densified daily observables; the results fluctuate depending on the algorithm tested. No approach turned out to be accurate or robust in all configurations. In this study the potential benefit of having a correct a-priori estimation of bathymetry was highlighted.

In the river hydraulics community, the most employed data assimilation studies are based on sequential algorithms, the Kalman filter and its variants: see Roux and Dartus, 2006; Ricci et al., 2011 based on the 1D Saint-Venant model, Munier et al., 2015 based on the diffusive wave model and Biancamaria et al., 2011; Yoon et al., 2012; Paiva et al.; Emery et al., 2017 for complete river networks using routing methods. In these studies, the sequential data assimilation

algorithms correct the upstream discharge (or potentially a constant roughness coefficient K). However none of these study address the challenging inference of the triplet, that is: the discharge Q, the bathymetry b and the roughness coefficient K.

The Variational Data Assimilation (VDA) approach, based on the optimal control of the dynamics flow model, see Sasaki, 1970; Le Dimet and Talagrand, 1986; Navon, 1998; Cacuci et al., 2013 and e.g. Bouttier and Courtier, 2002; Monnier, 2014 for on-line courses, has demonstrated to be an excellent approach to solve the present inverse problem. The VDA approach consists in minimizing a cost function measuring the discrepancy between the model outputs and the observations; somehow combining at best the model, the observations and prior information. This approach enables to "invert" high-dimensional unknown "vector of parameters" in complex dynamic models. This approach is operational in meteorology and oceanography since the beginning of the century. In river hydraulics, in some circumstances it is possible to infer the key unknown "parameters" of the flow model: the inflow discharge $Q_{in}(t)$, the bathymetry $b(x)$, the roughness K and/or forcing terms (e.g. lateral fluxes). Among the pioneer VDA studies dedicated to hydraulic models, let us cite Panchang and O'Brien, 1989; Chertok and Lardner, 1996; Sanders and Katopodes, 1999; next Bélanger and Vincent, 2005; Honnorat et al., 2006; Castaings et al., 2006 infered the inflow discharge in 2D shallow water river models.Infering the discharge and complete set of the hydraulic parameters (bathymetry, roughness) from WS measurements may be impossible, depending on the flow regime, the adequacy between the observations frequency and the flow dynamics, and the prior information. The related equifinality issues are highlighted e.g. in Aronica et al., 1998 in the calibration of spatially distributed roughness coefficients.

The inference of the key triplet (inflow discharge, effective bathymetry and friction coefficient) is investigated in Honnorat et al., 2009, 2010 but from surface Lagrangian drifting markers providing constraining observations. Based on a real river dataset (Pearl River in China), the upstream, downstream and a few lateral fluxes are identified from water levels measured at in-situ gauging stations in Honnorat et al., 2006; however again the bathymetry and roughness are given. The assimilation of spatially distributed water level observations in a flood plain (a single image acquired by SAR) and a partial in-situ time series (gauging station) are investigated in Lai and Monnier, 2009; Hostache et al., 2010, see also Monnier et al., 2016. In Gejadze and Monnier, 2007; Marin and Monnier, 2009 the inference of inflow discharge and lateral fluxes are identified by VDA by superposing a 2D local "zoom model" over the 1D Saint-Venant model; these studies are not conducted in a sparse altimetry measurement context.

The altimetry measurements of WS are generally sparse compared to the flow dynamics, both in space and time. This important feature of the inverse problem is analyzed in detail in Brisset et al., 2018 through the very instructive "identifiability map". The latter is the (x, t)-plane representation of all the available information, that are: the satellite measurements, the model response in terms of wave propagation and the misfit with respect to the equilibrium state. Concerning the bathymetry inference, it is shown in Gessese et al., 2011; Garambois and Monnier, 2015, see also Brisset et al., 2018, that given a single in-situ measurement of bathymetry, the complete bathymetry profile can be reconstructed. Gejadze and Malaterre, 2017; Oubanas et al., 2018; Brisset et al., 2018 present accurate inferences of $Q(t)$ by a similar VDA process as the present one but based on the 1D Saint-Venant flow model "only" (it does not include a hierarchical modeling strategy as in the present method). Moreover in the unique river case considered in Oubanas et al., 2018, a crucial prior information is implicitly imposed: the rating curve $Q(Z)$ applied at downstream is given (not as an unknown) hence controlling the flow. Such strong prior information makes converge the VDA process to the correct discharge $Q(t)$ and the bathymetry $b(x)$: the values corresponding to the imposed rating curve. (Observe that in Oubanas et al., 2018 the chosen first guess values of the VDA iterative process are a light Gaussian perturbation of the "true" values of (K, b) only). In summary these recently developed VDA algorithms are accurate to infer the inflow discharge $Q_{in}(t)$ but from accurate prior information. The latter may be a controlling downstream flow condition Gejadze and Malaterre, 2017; Oubanas et al., 2018 or a single depth measurement in the river portion Brisset et al., 2018.

In view to apply the algorithms to worldwide ungauged rivers no prior information may be introduced neither in the direct model nor in the inverse method. This was not the case up to now; this is a scenario considered in the present study which proposes improvements of the aforementioned VDA algorithms in few manners. Firstly the hierarchical modeling strategy strengthens the robustness of the estimations in particular if a mean value of Q is provided by a database or a large scale hydrological model (see e.g. Andreadis et al., 2013; Cohen et al., 2014; Allen and Pavelsky, 2015). Also, following Gessese et al., 2011; Garambois and Monnier, 2015; Brisset et al., 2018, if a unique reference depth value of the river is available, it is exploited in the inversion process too. These prior rough information are mathematically interpreted in the inversion algorithm; it turns out that the knowledge of a single mean value of a field (e.g. Q or b) improves the accuracy of the estimations of all the unknowns which are $(Q(t), b(x); K)$; K being set as a flow-dependent law.Of course if denser information is provided, in particular a good bathymetry profile provided e.g. by in situ measurements or penetrating Lidar in shallow zones (see e.g. Saylam et al. (2017)) then the inverse algorithm can be applied as it is.

The numerical results are presented on three rivers, ~ 100 km long each. Each case presents a "low identifiability index" (following the definition introduced in Brisset et al., 2018); that is a quite high frequency of hydrograph variations compared to the observation frequency; in short, challenging inverse dynamic flow problems.

Two scenarios of observation are considered: 1) a SWOT like Cal-Val orbit with $\sim$1 day period; 2) a SWOT like data with 21 days period (with 1 to 4 passes at mid-latitudes). For each river case and observation scenario, three

inverse problems are considered: the most challenging one, ungauged rivers observed by SWOT only; the second one where multi-temporal priors on discharge are available; and finally the third one where in-situ measurements of bathymetry are available. Suitable methods for each case were developed and are presented in this article. All the algorithms and methods developed here are available in the open-source computational software DassFlow (DassFlow, 2018).

The outline of the article is as follows. Section 2 presents the river flow models: the Saint-Venant equations with the particular cross section shapes and low Froude - low complexity systems (the latter are based either on the classical Manning-Strickler's law or on explicit "low Froude bathymetry" expressions). Section 3 presents the advanced VDA method taking into account prior hydraulic scale and error measurement amplitudes. The description of the three test rivers and scenarios (20 numerical experiments) are presented in Section 4. Moreover the first guess computation is described, depending on the available prior information. Section 5 focuses on hydraulic inferences on ungauged rivers; a discussion on the equifinality issue is proposed. The case where in-situ measurements are available, this could be a single bathymetry value or a few discharge values, is addressed in Section 6. Section 7 presents how to compute real-time estimations of discharge using the low complexity system, past the calibration - "learning" period. A conclusion is proposed in Section 8.

2 River flow hydrodynamic models

The primary (direct) river flow model is the classical Saint-Venant equations in $(A, Q)(x, t)$ variables (see e.g. Chow, 1964; Carlier, 1982) with the Manning-Strickler roughness coefficient K defined as a power law in water depth h. It is worth to recall that at the current hydrology satellites measurement scale, the river flows present a low Froude number F_r; typically F_r ranges approximatively within $[0.1, 0.3]$. A first consequence is that the imposed downstream condition controls the flow and in lack of prior information it is important that this condition is as "transparent" as possible. This is the case here since at downstream the normal depth is imposed from Manning's equation with friction slope equal to the bottom slope. A second consequence is the relatively good accuracy of the simple Manning-Strickler's equation to model the flow (see e.g. Durand et al., 2014; Garambois and Monnier, 2015; Durand et al., 2016 for studies in the present SWOT context). However the scalar standard equation is highly sensitive to uncertainties; moreover as highlighted in Garambois and Monnier, 2015 the actual independent variable is Q/K (and not Q). Then in this section "low complexity systems" are developed; they are based on the classical hydraulic assumption "low Froude" hence similar in this sense to the Manning-Strickler's equation (see e.g. Chow, 1964) but taking advantage of the WS measurements. These original systems are employed both for direct modeling (real-time estimations past the calibration period) and inverse modeling (e.g. estimation of the first guess in the VDA method). Their resolution is much more robust than the usual Manning-Strickler's equation.

2.1 The 1D Saint-Venant model

The 1D Saint-Venant equations are depth-integrated and rely on the long-wave assumption; that is the geometrical ratio of the flow $\varepsilon = h^*/L^*$ is small, h^* being a characteristic water depth and L^* a characteristic length scale (shallow water assumption, see e.g. Chow, 1964). In their non conservative form in (A, Q) variables, A the wetted-cross section $\left[m^2\right]$, Q the discharge $\left[m^3.s^{-1}\right]$, the equations read as follows (Chow, 1964):

$$\begin{cases} \partial_t(A) + \partial_x(Q) & = 0 \\ \partial_t Q + \partial_x\left(\frac{Q^2}{A}\right) + gA\,\partial_x Z & = -g\,A\,S_f(A, Q; K) \end{cases} \tag{1}$$

where g is the gravity magnitude $\left[m.s^{-2}\right]$, Z is the WS elevation $[m]$, $Z = (b + h)$ where b is the lowest bed level $[m]$ and h is the water depth $[m]$.

S_f is the classical Manning-Strickler friction term:

$$S_f(A, Q; K) = \frac{|Q|Q}{K^2 A^2 R_h^{4/3}} \tag{2}$$

with K the Strickler roughness coefficient $\left[m^{1/3}.s^{-1}\right]$, $R_h = {}^{A}/_{P_h}$ the hydraulic radius $[m]$, P_h the wetted perimeter. It will be noticed in next paragraph that R_h may be approximated by the water depth h for large rivers. The discharge Q is related to the average cross sectional velocity u $\left[m.s^{-1}\right]$: $Q = uA$. The Strickler roughness coefficient K is defined as a power law in h:

$$K(h) = \alpha\ h^{\beta} \tag{3}$$

where α and β are two constants. Similar approaches based on hydraulic geometry or power law resistance equations are developed in the literature for predicting mean flow velocity for example on a wide range of river measurements in

Bjerklie et al. (2005) or else for gravel bed streams in Ferguson (2010). The power law relation (3) enables to set the roughness in function of the flow regime; it is richer than a constant uniform value as it is often set in the literature from a-priori table of roughness in function of river types for instance (e.g. (Chow, 1959)).

At upstream the discharge $Q_{in}(t)$ is imposed. At downstream the Manning-Strickler equation depending on the unknowns $(A, Q; K)_{out}$ is imposed (it is classically integrated in the Preissmann scheme equations).The initial condition is set as the steady state backwater curve profile: $Z_0(x) = Z(Q_{in}(t_0))$. This 1D Saint-Venant model is discretized using the classical implicit Preissmann scheme (see e.g. Cunge et al., 1980). It is implemented into the computational software DassFlow DassFlow (2018).

2.2 River description from SWOT measurements

The forthcoming SWOT measurements will provide spatially distributed measurements of river surface elevation Z and width W with temporal revisits (Rodríguez, 2012). We denote by $(Z_{r,p}, W_{r,p})$ the WS elevation and width for reach r at the satellite overpass p instant. The SWOT WS slope will be calculated at the scale of reaches of several kilometers (see e.g. Frasson et al., 2017 on this point). The slopes are calculated by finite differences on Z.

We consider R reaches, $r = 1, .., R$, and $(P + 1)$ overpasses, $p = 0, .., P$. The overpasses are ordered by increasing flow height. The case $p = 0$ denotes the lowest water level. The SWOT data set on a river domain is: $\{Z_{r,p}, W_{r,p}\}_{R,P+1}$. The direct model (1) is considered with the specific cross-sectional geometry shape described in Fig. 1. It consists in discrete cross sections formed by asymmetrical trapezium layers $(Z_{r,p}, W_{r,p})$, the center ox each in the cross-flow direction being denoted by $Y_{r,p}$. In the following we assume that the WS slope is positive: $S_{r,p} = -\partial_r Z_{r,p} \geq 0$.

The cross-sectional areas $A_{r,p}$ are defined as follows: $A_{r,p} = A_{r,0} + \delta A_{r,p} = A_{r,0} + \int_{h_0}^{h_p} W_r(h)dh \ \ \forall r \ \forall p$. The variations $\delta A_{r,p}$ are approximated by the trapeziums $\delta A_{r,p} \approx \sum_{q=1}^{p} \frac{1}{2}(W_r^q + W_r^{q-1})(h_r^q - h_r^{q-1})$. The lowest cross-sectional areas denoted by $A_{r,0} \forall r$ are unobserved; they are key unknowns of the flow model. They are represented by rectangles, see Fig. 1, or any other fixed shape e.g. a parabola; all the other cross-sectional areas are trapezoidal.

We have: $h_{r,p} \approx R_{r,p}^h \approx \frac{A_{r,p}}{W_{r,0}+2h_{r,p}+W_{r,p}} \ \ \forall r$. It is worth to point out that this approximation has been numerically verified on all considered rivers. Since $W >> h$, it follows the effective depth expression: $h_{r,p} = (A_{r,0} + \delta A_{r,p})(W_{r,0} + W_{r,p})^{-1}$. The flows are supposed to be gradually varied that is: $\partial_x W_{r,p}/W_{r,p} \approx 0$.

The unobserved wetted cross section A_0 can be represented by a rectangle, a trapezium, a parabola or even a triangle, by setting: $A_0 = \alpha_A h_{0,\alpha} W$ with $\alpha_A \in [\frac{1}{2}, 1]$. However it will be shown that the a-priori effective cross-section shape does not influence the low Froude ("low complexity") flow relations, see Section 2.3. We define the hydraulic mean depth h_0 by: $h_0 = \frac{A_0}{W}$; it is the depth corresponding to an effective rectangular cross-section.

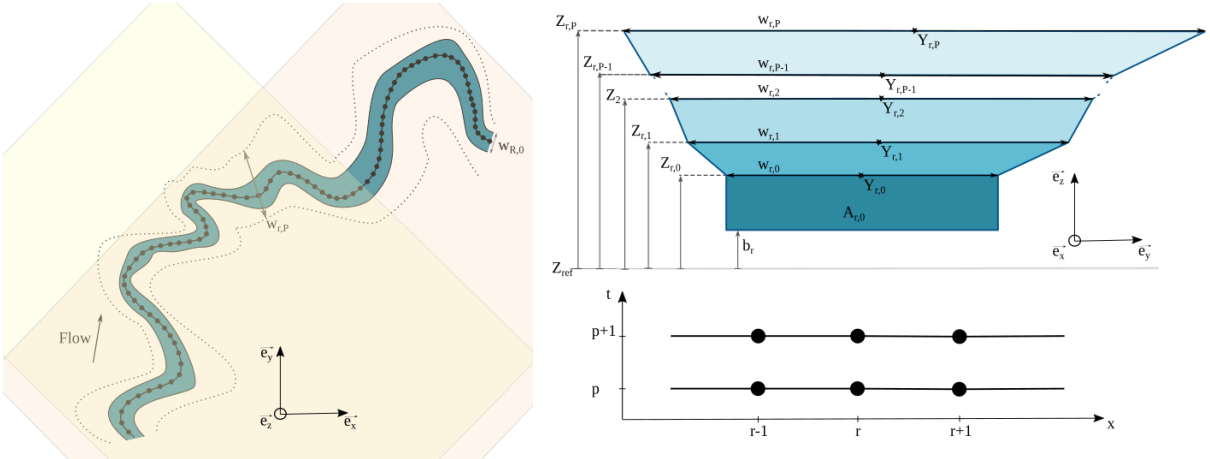

Figure 1: (Left) Schematic river plane view with satellite swaths (large colored rectangles), longitudinal grid with 1D averaged satellite measurements (black dots) along the river centerline (black line). (Right Top) Effective river cross section at reach r defined from SWOT data set $\{Z_{r,p}, W_{r,p}\}_{R,P+1}$. (Right Bottom) Space - time stencil (r, p). x denotes the curvilinear abscissa along the river centerline defined at low flow by $Y_{r,0}$ with $Y_{r,p}$ the middle of the cross sectional width.

2.3 Low complexity systems

In this paragraph, "low complexity" systems are derived; the terminology "low complexity" is in comparison with the space-time dependent Saint-Venant equations which require relatively high CPU time computations. On the contrary these low complexity systems will be computable in real-time. These systems are based on classical hydraulic

assumptions but they are derived in the particular present context: the assimilation of SWOT altimetry data. The three basic assumptions are the following.

A1) The altimetry measurements are relatively "large scale" compared to the river flows dynamics. In terms of temporal dynamics, since the satellite cannot make infer dynamics much faster than its own frequency revisit (which is $\approx$ 10 days), at each observation instant p, the flow may be described as a *steady state flow*. In terms of spatial variations, the SWOT instrument will provide an average value of the WS measurement at $\sim$ 200 m reach long (RiverObs measurements, see (Frasson et al., 2017)); therefore the flow may be described as *locally uniform at the "reach length scale"*.

A2) At the reach scale defined above, the flow presents low Froude number values. Under the *low Froude flow assumption,* the inertial terms in the momentum equations can be neglected.

A3) The considered rivers do not present lateral fluxes.

Moreover as already mentioned the considered rivers are wide enough to assume that the hydraulic radius $R_h \approx h$ in the Manning-Strickler friction term S_f, see (1).

2.3.1 The low Froude system: local Manning-Strickler's laws

For a rectangular cross section, the Froude number Fr satisfies: $Fr^2 = uc_e^{-1}$ with c_e the wave celerity, $c_e = \sqrt{gh}$. Assuming that the flow is permanent and low Froude, $Fr^2 << 1$, the momentum equation simplifies as the Manning-Strickler law: $Q = KAh^{2/3}\sqrt{S}$. Considering this law at each river reach r and each observation time p, this provides the following system:

$$(K_{r,p}^{-1}Q_{r,p})^{3/5} = (A_{0,r} + \delta A_{r,p})W_{r,p}^{-2/5}S_{r,p}^{3/10} \ \forall r, \forall p \tag{4}$$

for each reach $r \in [1...R]$ and each satellite pass $p \in [0...P]$. The terms $\delta A_{r,p}, W_{r,p}, S_{r,p}$ are measured, while the terms $Q_{r,p}, A_{0,r}$ and $K_{r,p}$ are not.

This system (4) can be employed differently depending on the available information and the unknowns. In the inversion computations presented in Section 6.2, (4) is reformulated in (14) to estimate pairs ($K_r^{3/5}$, $A_{r,0}$) from prior discharge values $Q_{r,p}$ (ancillary data).

2.3.2 The "low Froude" bathymetry

By injecting the expression of Q in (4) (we skip the subscripts $_{r,p}$) into the mass conservation equation ($\partial_x Q = 0$), it follows: $\partial_x \left(KAh^{2/3}S^{1/2}\right) = 0$. Assuming a constant roughness coefficient K, this simplifies to: $\frac{\partial_x h}{h}(x) = -\frac{3}{2}\left(\frac{\partial_x (S^{1/2})}{S^{1/2}} + \frac{\partial_x A}{A}\right)(x)$.

Next, following Gessese et al., 2011 and given a reference depth value h_{ref} (measured at one reference reach ref), the explicit expression of h follows: $h(x) = h_{ref}\left(AS^{1/2}\right)_{ref}^{3/2} \cdot \left(AS^{1/2}\right)^{-3/2}(x)$. This estimation of water depth h is analyzed in detail in Gessese et al., 2011; Garambois and Monnier, 2015.

Let us extend this estimation of the water depth h (hence the bed elevation b) to the present context, that is from a complete set of WS measurements. If considering an effective cross-sectional area $A = \alpha_A hW$ with $\alpha_A \in [\frac{1}{2}, 1]$ then the bathymetry expression reads: $b(x) = Z(x) - C_{ref} \cdot \alpha_A^{-3/5}(x) \cdot (WS^{1/2})^{-3/5}(x)$ with $C_{ref} = h_{ref}\left(\alpha_A WS^{1/2}\right)|_{ref}^{3/5}$. The three parameters (α_A, W, S) describe the three dimensions of the flow.

Given the WS measurements (Z, $WS^{1/2}$) and the value S_{ref} at an arbitrary reach ref, this explicit expression of $b(x)$ provides an effective bathymetry. Observe that the effective bathymetry elevation b is equivalent if considering different wetted cross-section shapes determined by α_A. In other words, in the present low Froude relations, the shape of the effective cross-sectional area A may be chosen arbitrarily. In the following we set $\alpha_A = 1$; that is a rectangular effective shape. Finally the effective bathymetry expression under the assumptions A1)-A3) previously mentioned reads:

$$b_r + (Z_{ref,p} - b_{ref}) \cdot \mathcal{O}_{ref,p}^{-1} \cdot \mathcal{O}_{r,p} = Z_{r,p} \ \forall r, \ r \neq ref, \ \forall p \geq 0 \tag{5}$$

with the observational term $\mathcal{O}_{r,p} = \left(W_{r,p}\sqrt{S_{r,p}}\right)^{-3/5} \ \forall r \, \forall p$. (The only observational terms of this estimation are Z and the product $WS^{1/2} \equiv \mathcal{O}$).

In the following the bathymetry $\{b_r\}_r$ solution of (5) is called the "Low Froude bathymetry".

The system (5) contains $(P+1)\times(R-1)$ equations (given 1 reference reach only) with R unknowns: the bathymetry vector $b = (\{b_r\}_r, b_{ref})$ $r \in [1, R]\,, r \neq ref$. The system reads: $(A.b)_p = (F)_p \ \forall p$, with$(F_r)_p = Z_{r,p} - Z_{ref,p}\mathcal{O}_{ref,p}^{-1} \cdot \mathcal{O}_{r,p}$ and the $(R-1)(P+1) \times R$ matrix $(A)_p = \left[I_{(R-1\times R-1)}|\mathcal{O}_{ref,p}^{-1} \cdot \mathcal{O}_{r,p}\right]$. For $P \geq 1$, A is of maximal rank excepted if the observational vectors $(\mathcal{O}_r)_p$ are linearly dependent; that is not the case if the considered water flow lines represent flow variations.

On the coupled influence between b and a non constant roughness coefficient K. As shown above and already demonstrated in Gessese et al., 2011; Garambois and Monnier, 2015, the low Froude assumption enables to separate

the bathymetry effect from the friction effect *if* the friction coefficient K is constant, see (5); K does not appear anymore in (5). On the contrary, if K varies in space or depends on the depth h, like in (3) or in the Einstein formula (see e.g. Chow, 1964) then K and b have a coupled influence even at low Froude. Typically if considering the following power-law: $K(h) = K_0 \cdot (h - h_0)^\beta(x)$ with gradually varied coefficients i.e. $\partial_x K_0 \sim 0 \sim \partial_x \beta$, after calculations the depth expression reads: $[h(x) \cdot |h(x) - h_0|^{3\beta/2}] = c_0 \cdot (AS^{1/2})^{-3/2}(x)$ with $c_0 = |h_{ref} - h_0|^{3\beta/2} \cdot h_{ref} \cdot (AS^{1/2})_{ref}^{+3/2}$ (h_{ref} the reference depth value). The case K constant is recovered from the equation above by setting $\beta = 0$.

Relationship with empirical laws. It may be practical to consider empirical laws based on hydraulic geometry (see e.g. Leopold and Maddock, 1953) such as: $Z_{r,p} = b_r + a_r {W_{r,p}}^\beta$. In other respects, (5) re-writes as follows: $Z_{r,p} = b_r + C_{ref,p} \cdot \alpha_{A,r}^{-3/5} \cdot (WS^{1/2})|_{r,p}^{-3/5}$ $\forall r,\ \forall p,\ p = 0, .., P$ with $C_{ref,p} = h_{ref,p} \left(\alpha_A W S^{1/2}\right)_{ref,p}^{3/5}$. We assume constant cross section shapes ($\alpha_{A,r} = \alpha_A\ \forall r$). By equaling the two estimations it follows: ${W_{r,p}}^\beta \cdot (W_{r,p} S_{r,p}^{1/2})^{3/5} = a_r^{-1} \cdot h_{ref,p} \left(WS^{1/2}\right)_{ref,p}^{3/5}$ $\forall r\ \forall p$. Assuming that the flow is uniform in terms of the observational term ($WS^{1/2}$) i.e. this quantity is constant for the considered reaches, we obtain that: $W_p^\beta = a^{-1}\ h_p$; equivalently: $Z_p = b + a\ W_p^\beta$. Therefore the low Froude estimation (5) contains empirical laws of the form indicated above. Given β and time series of WS elevation and width this relation allows to infer an effective river bed elevation as suggested by Bjerklie et al., 2018. with $\beta = 2$. Such law could be defined in function of hydraulic geometry knowledge (see e.g. Leopold and Maddock, 1953). The relationship along a reach between hydraulic geometry coefficients (Gleason and Smith, 2014) could also be investigated in the light of geomorphological variability.

On the accuracy of these low Froude - low complexity systems. The two systems (4) and (5) turn out to be reasonably accurate in the present altimetry context, see assumptions A1)-A3). Their solutions have been numerically assessed in detail in Garambois and Monnier, 2015 and in the present precise context too, see the numerical results in Section 6.

3 The Variational Data Assimilation (VDA) formulation

Given the WS measurements, the VDA method aims at estimating the "input parameters" of the Saint-Venant flow model that is: the inflow discharge $Q_{in}(t)$ of the Saint-Venant model, the bathymetry $b(x)$ and the friction coefficient $K(h)$, see (3). In discrete form, this unknown "parameter" reads:

$$c = (Q_{in,0},\ ...,\ Q_{in,P};\ b_1,\ ...,\ b_R;\ \alpha,\ \beta)^T \tag{6}$$

The subscript p denotes the instant, $p \in [0..P]$, r denotes the reach number, $r \in [1..R]$, see Fig. 1 and α and β are the law parameters defined by (3). Since the relation between the elevation Z and the cross-sectional area A (see the river description section 2.2) defines a bijection function (a one-to-one correspondence), measuring Z is equivalent to measuring A. Of course the parameters used for imposing a normal depth at downstream, see Section 2.1, are considered as unknown.

A cost function denoted by j is defined as:

$$j(c) = j_{obs}(c) + \gamma\, j_{reg}(c) \tag{7}$$

The term $j_{obs}(c)$ measures the misfit between the observations and the model output:

$$j_{obs}(c) = \frac{1}{2} \left\| (Z(\mathrm{c}) - Z_{obs}) \right\|_N^2 \tag{8}$$

The norm N is defined from the a-priori covariance operator N: $\|\cdot\|_N = \|N^{1/2} \cdot\|_2$; N is a positive definite matrix. The term $j_{reg}(c)$ is the so-called "regularization term"; it is discussed below. The coefficient γ is a weighting coefficient, $\gamma > 0$.

The WS elevation Z depends on c through the flow model (1). The inverse problem reads as: $c^* = \mathrm{argmin\ j(c)}$. It is an optimal control problem of (1) (Lions, 1971). It is classically solved by a Quasi-Newton descent algorithm, here the L-BFGS algorithm presented in Gilbert and Lemaréchal, 1989. This first order method requires the computation of the cost gradient $\nabla j(c)$. This optimization problem is a VDA formulation (see e.g. Le Dimet and Talagrand (1986); Bouttier and Courtier (2002); Monnier (2014); Cacuci et al. (2013)).

The gradient is computed by introducing the adjoint model, hence enabling to consider large control vector dimensions. The adjoint code is obtained by employing the automatic differentiation tool Tapenade (Hascoët and Pascual, 2013). We refer to Monnier et al., 2016; Monnier, 2014; DassFlow, 2018 for detailed know-hows and their implementation.

The unknown parameter c contains three variables of different physical nature which are space and/or time dependent. Moreover the bathymetry $b(x)$ and the friction coefficient $K(h)$ are correlated and they may have a similar influence in terms of WS signature therefore leading to an ill-posed inverse problem (see Garambois and Monnier, 2015 for

such a discussion in the present inversion context). Then the inverse problem needs to be "regularized" otherwise a few optimal solutions c^* may minimize j but without being the "true" ones: that is the equifinality issue (see e.g. Kaltenbacher et al., 2008 for details on the theory of regularization of ill-posed inverse problems).

The present VDA formulation is regularized in two ways. Firstly, the additional term j_{reg} is introduced in the cost function, see (7). It is called the regularization term) and it is defined by: $j_{reg}(c) = \frac{1}{2}\left\|b"(x)\right\|_2^2$. Therefore j_{reg} imposes a simple smoothing effect on the infered bathymetry profiles $b(x)$. Next to solve much more efficiently this ill-posed inverse problem some covariance operators are introduced.

Covariance operators and change of control variable.

Following Lorenc et al., 2000, we make the change of variable:

$$k = B^{-1/2}(\mathrm{c} - \mathrm{c}_{prior}) \tag{9}$$

where B is a covariance matrix. Recall that the unknown parameter (the control variable) c is defined by (6); c_{prior} is a prior value (also called "background" or "first-guess" value). The value of c_{prior} will depend on the context and the information a-priori available.

The choice of B also represents an important prior information since the computed optimal solution k^* depends on B. Indeed, after this change of variable, the optimality condition reads: $B^{1/2}\nabla j(c) = 0$. This change of variable may be viewed as a preconditioning method (see e.g. Haben et al., 2011a,b for detailed analysis). Then the new optimization problem to be solved reads:

$$\min_k \mathrm{J}(k) \tag{10}$$

with $\mathrm{J}(k) = j(c)$, j defined by (7) and the control vector k defined by (9). The unknown parameter k contains the three variables $Q_{in}(t)$, $b(x)$, $K(h)$ (in their discrete form). These three variables are assumed to be uncorrelated: B is defined as a block diagonal matrix. We set:

$$B = \begin{pmatrix} B_Q & 0 & 0 \\ 0 & B_b & 0 \\ 0 & 0 & B_K \end{pmatrix} \tag{11}$$

Each block $B_\square$ is defined as a covariance matrix (positive definite matrix). The matrices B_Q and B_b are set as classical second order auto-regressive correlation matrices (see e.g. Lorenc et al., 2000; Haben et al., 2011b; Tarantola, 2005):

$$(B_Q)_{i,j} = (\sigma_Q)^2 \exp\left(-\frac{|t_j - t_i|}{\Delta t_Q}\right) \text{ and } (B_b)_{i,j} = (\sigma_b)^2 \exp\left(-\frac{|x_j - x_i|}{L_b}\right) \tag{12}$$

The parameters Δt_Q and L_b act as correlation wave lengths. Given the observation frequency (1 day minimum), given the measurements accuracy (200m long "observation pixels") and given the typical Froude number of the observed river flows, adequate values for these parameters are: $\Delta t_Q = 24$ h and $L_b = 1$ km. We refer to Brisset et al., 2018 for a thorough analysis of the discharge inference in terms of frequencies and wave lengths. The matrix B_K is diagonal; it is set as: $B_K = diag(\sigma_\alpha^2, \sigma_\beta^2)$. The four scalar values $\sigma_\square$ may be viewed as variances; their values are detailed in the numerical results section.

Finally, the VDA formulation above takes into account prior hydraulic scales (the parameters Δt_Q and L_b) and error measurement amplitudes (the parameters $\sigma_\square$).

4 Test rivers and data description

In this section are presented a description of the three test rivers and the different scenarios depending on the availability of data. The developed methods to compute the first guesses (estimations used as the first value in the iterative VDA process) are detailed; a summary of all experiments is presented too.

4.1 River cases and Water Surface (WS) measurements

The inference capabilities of the VDA algorithm and the low complexity relations previously introduced are assessed on three rivers with two densities of WS observations representing increasing difficulty. They consist in 75km of the Garonne River (France), 98km of the Po River (Italy) and 147km of the Sacramento River (California, USA), see Table 1 for details. These three rivers have contrasting morphological characteristics in terms of the average variability of the slope and the shape of the cross section, resulting in hydrodynamic nonlinearities observable in WS signatures. Moreover the Po and Garonne rivers hydrographs represent two orders of magnitude of discharge with mean flows of $156m^3/s$ and $1499m^3/s$ respectively (Table 1). The impact of WS measurements sampling on hydraulic controls identifiability is assessed with a SWOT Cal/Val scenario with daily observations on the Po and Garonne Rivers, and with the nominal SWOT spatio-temporal sampling, i.e. the most difficult case, on the Sacramento River.

The SWOT-like WS observations used in the following VDA experiments consist for each river in sets of $(Z_{r,p}, W_{r,p})_{R,P+1}$. The Sacramento river was the only case for which SWOT Hydrology Simulator outputs were available. In order to conduct the present numerical experiments, SWOT-like data have been simulated (with Gaussian errors added) on the two other rivers: Garonne and Po Rivers. The synthetic data are as follows: $Z_{obs}(x,t) = Z_{true}(x,t) + \mathcal{N}(0, \sigma_Z)$ with $\sigma_Z = 25$ cm corresponding to the expected magnitude of SWOT measurement errors at the present spatial scale - according to the SWOT scientific requirements (Rodríguez, 2012). Also we set $\Delta t_{obs} = 1$ day, that is a revisit frequency corresponding to the calibration/validation (Cal/Val) phase of the SWOT mission. For the Sacramento case, the observability corresponding to a nominal 21 days SWOT cycle is simulated by the SWOT Hydrology Simulator. The whole reach is observed by SWOT (tracks number #249 and #527 respectively) at day 9 and 19 for each 21 days repeat cycle; the simulated measurement error on Z is characterized on average by a variance $\sigma_Z = 34$ cm, see Tab. 1. We think that it is interesting to use this higher (simulated) measurement error, in case the real SWOT errors would be locally higher than scientific requirements, but more importantly because it represents a supplementary difficulty for the inference. Finally the spatial sampling is similar for the three cases with a fixed spatial sampling $\Delta x_{obs} = 200$ m for the Garonne and Po Rivers and for the Sacramento River, the SWOT Hydrology Simulator outputs are averaged in space on ~ 200 m nodes (i.e. RiverObs node average spacing).

Table 1: Hydraulic characteristics for each case

Case Name	Reach Length (km)	Max. Width (m)	Avg. Slope (m/km)	Avg. Flow (m3/s)	Froude Range (-)
Garonne (US)	75	49/1,383	0.861	156	0.03-0.67
Po	98	116/5,515	0.145	1499	0.04-0.47
Sacramento	147	59/678	0.558	251	0.02-0.64

Table 2: Observations sources and characteristics for each case

Case Name	Hydrodynamic Model	Temporal Window	Observations Frequency	Reference
Garonne (US)	HEC-RAS	06 jan. 2010 - 06 avr. 2010	1 day	Larnier, 2010
Po	HEC-RAS	01 jan. 2002 - 01 avr. 2002	1 day	Di Baldassarre et al., 2009
Sacramento	HEC-RAS + SWOT HR	01 jan. 2009 - 27 jun. 2009	21 days	Rogers, 2014

4.2 Classes of inverse problems for ungauged and poorly gauged rivers

The future SWOT mission will observe worldwide rivers wider than 100 m with on average 1 to 4 temporal revisits every 21 days at mid-latitudes, see e.g. Biancamaria et al., 2016. Given a river, the difficulty of the inverse problem previously described depends on the availability or not of ancillary data. The inversion capabilities of the algorithms and relations proposed in this article are tested on three scenarios of increasing difficulty. All scenarios are based on a set of SWOT observations consisting in measurements of river surface deformations $(Z_{r,p}, W_{r,p})_{R,P+1}$. These scenarios present a decreasing complexity in the sense the first one, the most challenging, considers SWOT data only, the last one, the easiest one, considers additional informative in-situ data. For each river case these three scenarios, based on SWOT data either with Cal/Val daily revisits or a nominal SWOT orbit, see Section 4.1 and Table 2, depend on the availability or not of in-situ / ancillary data:

1. Only SWOT observations are available, which corresponds to the most challenging inverse problem on ungauged rivers. This case is addressed in Section 5
2. SWOT observations and multi-temporal priors on discharge are available. These prior rough values (potentially a unique one) may be provided by worldwide hydrological models or discharge databases. This case is addressed in Section 6.
3. SWOT observations and one in-situ measurement of bathymetry (denoted by b_{ref}) is available. In this case an accurate effective bathymetry around (± 100 km) the reference value b_{ref} can be inferred. This case is addressed in Section 6.

For all scenarios and river cases a worldwide river database - the SWOT river database (Andreadis et al., 2013; Cohen et al., 2014; Allen and Pavelsky, 2018) in construction - contains (among other variables coming from databases described in references) at least one discharge value (inter-annual average value of discharge modeled with a large scale water balance model or estimated from ancillary hydrological databases) and one roughness estimate. Given the $R \times (P+1)$ WS observations, the complete control vector c formed by $(P+4R+2)$ unknowns, see (6), is computed by VDA. It is formed by $(P+1)$ unknown discharges, $4R$ unknown river bed elevations and a roughness parameterization depending on forward model state and two parameters (constants).

4.3 First guess computation

In order to be as realistic as possible, first guesses of the VDA process are infered from available worldwide databases and/or hydrological models. However for many rivers worldwide in-situ measurements will not be accessible or even do not exist. First guess values $c^{(0)} = \left(Q_{in,0}^{(0)}, ..., Q_{in,P}^{(0)}; b_1^{(0)}, ..., b_R^{(0)}; \alpha^{(0)}, \beta^{(0)}\right)^T$ of the parameter vector, see (6) and (9), are obtained as follows:

- At inflow, we set: $\forall p \in [0...P]$, $Q_p = Q_{MAF} \equiv Q_{in,0}^{(0)}$. Q_{MAF} is obtained by retrieving Mean Annual Flow (MAF) either from the SWOT a-priori river database (Andreadis et al., 2013; Cohen et al., 2014; Allen and Pavelsky, 2015) or from the global Water Balance Model (Wisser et al., 2010). So far, the WBM discharge is preferred in the SWOT discharge community as a reference.
- A constant prior on Manning-Strickler roughness coefficient $K^{(0)}$ is estimated from the SWOT a-priori river database under construction (see (Andreadis et al., 2013; Cohen et al., 2014; Allen and Pavelsky, 2018)). The $K^{(0)}$ values in the present case are 25, 33 and 25 respectively for the Garonne, Po, and Sacramento rivers (i.e. the $\alpha^{(0)}$ values with $\beta^{(0)} = 0$, see (3)).
- A prior on the unobserved low flow $b^{(0)}$ (or equivalently the low flow cross sectional areas $(A_{r,0})_r$ assuming a shape and knowing the low flow WS widths $(W_{r,0})_r$, see Section 2.3) can be obtained by the following three methods (see Table 3).
  - *"Manning"* - the unobserved low flow bathymetry $b^{(0)}$ is obtained by inverting the Manning equation (4) applied to a single flow line with $K^{(0)}$ and Q_{WBM} constant in space and time,
  - *"Manning-multi"* - low flow bathymetry $b^{(0)}$ is obtained by inverting Eqn (13) with numerous flow lines that represent a large range of flow regimes and variabilities on the studied river. In that case, flow lines can be grouped by deciles and put in correspondence with deciles of discharge from the worldwide available WBM model or a discharge database.
  - *"Low Froude"* - In the case where one bathymetry measurement is available, an effective bathymetry is derived from WS observables and the low Froude equation (5).

For the three scenarios, *"Manning"*, *"Manning-multi"* and *"Low Froude"*, the first-guesses $Q^{(0)}$, $\alpha^{(0)}$ and $\beta^{(0)}$ are determined using the same methods described above. Only the method used to compute $b^{(0)}$ differs for each scenario.

It is important to point out that if $b^{(0)}$ is estimated from the simple one-value Manning-Strickler relation, this first crucial estimation of the bathymetry is highly sensitive to any error made on the a-priori estimation of $(Q^{(0)}, K^{(0)})$.

These three scenarios are tested on all river cases, either with perfect or noisy observations, except for the Sacramento River were the second scenario cannot be computed. Indeed the small number of overpasses (17) is not sufficient to determine flow regimes an thus statistically relate observations with deciles of discharge in databases.

The cost functions used to evaluate the performance of inversions at assimilation times consists in classical $RMSE = \sqrt{\frac{\sum_{t=1}^{n}(Q_t^{est} - Q_t^{true})^2}{n}}$ and relative RMSE $rRMSE = \sqrt{\frac{1}{n}\sum_{t=1}^{n}\left(\frac{Q_t^{est} - Q_t^{true}}{Q_t^{true}}\right)^2}$ where Q_{in}^{est} (resp. Q_{in}^{true}) is the estimated/infered (resp. observed) inflow discharge of size n in time.

5 Hydraulic inferences from WS long time-series on ungauged rivers

This section presents the numerical inference of the complete control vector (6) in the 1D Saint-Venant model (1) in the case of ungauged rivers where only WS observations distributed in space and time (SWOT like data) are available. The inferences are performed in the SWOT Cal/Val scenario for the Po and Garonne rivers and for a real like SWOT scenario on the Sacramento River. In this case, a preliminary analysis of the inverse problem and the redefinition of temporal controls based on the identifiability map is presented following Brisset et al., 2018. Finally, based on the obtained numerical results and an original mathematical development in the 1D Saint-Venant equations, a discussion on the equifinality issue is proposed.

5.1 SWOT Cal/Val scenario: Po and Garonne rivers

In this section a SWOT Cal/Val data context with daily measurements is considered (see section 4.2); the hydraulic optimization problem solved by VDA is started from a prior control vector $c^{(0)}$ infered from worldwide available databases. The latter are used to infer a prior roughness $K^{(0)}$ and bathymetry $b^{(0)}$ (*"Manning"* or *"Manning-multi"*) as explained above (Section 4.1). For each of the three river cases, a set of water elevations and width $(W, Z)_{R,P+1}$ measurements is considered for R reaches and $(P+1)$ revisits. The complete set of river parameters $c = (Q_{in,0}, ..., Q_{in,P}; b_1, ..., b_R; \alpha, \beta)^T$ is sought by minimizing (10), the inverse problem described in Section 3.

Table 3: Summary of experiments (*: two overpasses at days 9 and 19 every 21 days repeat period)

Experiment	River	$b^{(0)}$	Δx_{obs}	Δt_{obs}	$\sigma_Z^{perturb}$	σ_Z	σ_Q	σ_{α_K}	σ_{β_K}	σ_b
A.1	Garonne	Manning	200 m	1 day	0	25 cm	15 m3/s	0.5	0.01	25 cm
A.2	Garonne	Manning-multi	200 m	1 day	0	25 cm	15 m3/s	0.5	0.01	25 cm
A.3	Garonne	Low Froude	200 m	1 day	0	25 cm	15 m3/s	0.5	0.01	25 cm
A.4	Garonne	Manning	200 m	1 day	25 cm	25 cm	15 m3/s	0.5	0.01	25 cm
A.5	Garonne	Manning-multi	200 m	1 day	25 cm	25 cm	15 m3/s	0.5	0.01	25 cm
A.6	Garonne	Low Froude	200 m	1 day	25 cm	25 cm	15 m3/s	0.5	0.01	25 cm
B.1	Po	Manning	200 m	1 day	0	25 cm	71 m3/s	0.5	0.01	25 cm
B.2	Po	Manning-multi	200 m	1 day	0	25 cm	71 m3/s	0.5	0.01	25 cm
B.3	Po	Low Froude	200 m	1 day	0	25 cm	71 m3/s	0.5	0.01	25 cm
B.4	Po	Manning	200 m	1 day	25 cm	25 cm	71 m3/s	0.5	0.01	25 cm
B.5	Po	Manning-multi	200 m	1 day	25 cm	25 cm	71 m3/s	0.5	0.01	25 cm
B.6	Po	Low Froude	200 m	1 day	25 cm	25 cm	71 m3/s	0.5	0.01	25 cm
C.1	Sacramento	Manning	200m	21 days*	0	25 cm	20 m3/s	0.5	0.01	25 cm
C.2	Sacramento	Low Froude	200m	21 days*	0	25 cm	20 m3/s	0.5	0.01	25 cm
C.3	Sacramento	Manning	200m	21 days*	34 cm	25 cm	20 m3/s	0.5	0.01	25 cm
C.4	Sacramento	Low Froude	200m	21 days*	34 cm	25 cm	20 m3/s	0.5	0.01	25 cm

Two SWOT temporal samplings are considered, corresponding to the two successive phases of the future SWOT mission. First a Cal/Val scenario with daily observations on the Po and Garonne Rivers representing two orders of magnitude of discharge; second a real SWOT scenario on the Sacramento River are investigated with 2 observations for each 21 days period. The performances on river parameters inference, with various combinations of first guesses and observational sparsities are summed up in Table 5. In a SWOT measurement context, we denote by δ the noise level such that for all locations $\|Z_{obs} - Z_{true}\|^2 \leq \delta$ with Z_{obs} the observed and Z_{true} the true WS elevation. It is important in a noised observation context to avoid overfitting the data which can impact the infered parameters. A common technique used in the context of Tykhonov's regularization of ill-posed problems is Morozov's discrepancy principle, (see e.g. Kaltenbacher et al. 2008 and references therein): the regularization parameter γ, see (7), is chosen *a-posteriori* such that j does not decrease below the noise level. In the present numerical experiments, the convergence is stopped if $j_{obs}(c) \leq \chi\delta$ with $\chi \sim 0.9$.

Thanks to the regularization technique and the covariance operators introduced in the VDA formulation (see Section 3) the iterative process is relatively fast and robust, see the good performances in Table 5. For the 16 inverse computations (10 ungauged cases) performed, the misfit with the observations is greatly decreased.

5.2 SWOT Cal/Val scenario: Po and Garonne rivers

The inflow discharge hydrograph infered by VDA on the Garonne and Po Rivers are shown in purple on Fig. 2 (Scenarios A.4 and B.4 in Table 3). For each river the true daily inflow hydrograph over 90 days (green curve) is satisfactorily retrieved with $rRMSE_Q = 24.3\%$ on the Po River the and $rRMSE_Q = 9\%$ on the Garonne River at assimilation points (corresponding to observation points) - 8.5% and 4.8% respectively with perfect observations. The discharge inference is accurate despite the daily measurement errors. Concerning the bathymetry, the results are listed in Table 5 and plotted on Fig. 5 using B^* (deviation from the trend) for better reading. The estimated bathymetry $b_{1..R}$ is improved by the VDA process on the Garonne River (prior $RMSE_{b^{(0)}} = 0.39$ decreases to $RMSE_b = 0.31$) ; it remains close to the first guess in the Po River case. Let us recall that the roughness parameter K is model-equations-geometry dependent; its calibrated value compensates various modeling errors.

For both rivers considered as ungauged i.e. with prior $c^{(0)}$ defined from databases (scenarios A4,5 ; B4,5 and A1,2 ; B1,2 with perfect observations, Table 5), the inference of discharge remains robust and accurate. Most of the identification errors are absorbed by the roughness coefficient. Despite the improvement of robustness of the present enriched VDA method, some equifinality may remain between the bathymetry and the roughness. Indeed, on the Po River while discharge is very well retrieved, neither the bathymetry nor the roughness coefficient is significantly improved by the VDA process. An infinity of roughness and bathymetry values (embedded in the friction source term of the Saint-Venant equations) can mathematically produce the correct discharge given a flow stage. However the optimal value of the pair $(b(x), K)$, in the sense of the optimization problem (10), can be refined thanks to the low complexity relations presented in Section 7, see Table 5.

The "*Manning*" method has been performed using both the WBM discharge (Wisser et al., 2010) and the discharge from the SWOT a-priori river database (Andreadis et al., 2013; Cohen et al., 2014; Allen and Pavelsky, 2015) (respectively cases A.1.a, A.4.a, B.1.a and B.4.a; or A.1.b, A.4.b, B.1.b and B.4.b in Table 4). Recall that the "*Manning*" method used to determine the prior value of $b^{(0)}$ is based on a single pair $(Q^{(0)}, K^{(0)})$, therefore it is highly sensitive to any error in these first-guess values.

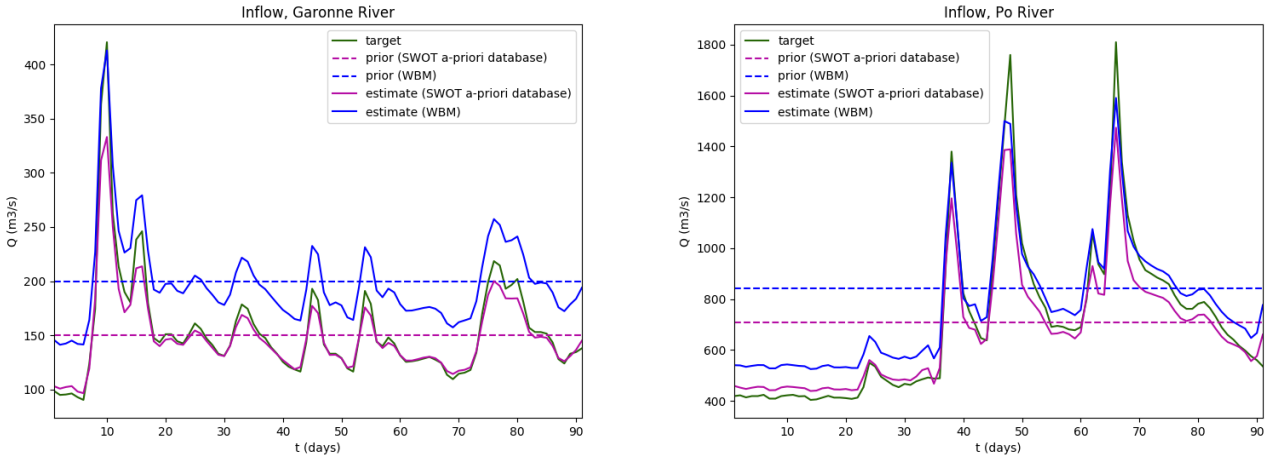

Figure 2: Inflow discharge (true=target, prior, infered=estimate) with daily SWOT-like observations. (Left) Garonne River Case A.3. (Right) Case B.3

Table 4: Scores of the inversions performed from different priors ("a" for SWOT a priori database, "b" for WBM) defining the hydrograph first guess $Q^{(0)}$.

Case	River	σ_Z^{obs}	Q_{prior} (m^3/s)	$RMSE_{b^{(0)}}$ (m)	$RMSE_Q$ (m^3/s)	$rRMSE_Q$ (%)	$rRMSE_{Q*}$ (%)	$RMSE_b$ (m)
A.1.a	Garonne	0	150	0.18	13.4	5.1	5.0	0.43
A.1.b	Garonne	0	270	0.51	40.6	30.5	7.5	0.73
A.4.a	Garonne	25 cm	150	0.39	24.0	10.3	9.8	0.31
A.4.b	Garonne	25 cm	270	0.54	41.8	33.0	13.3	0.45
B.1.a	Po	0	710	0.61	83.9	8.5	8.5	0.75
B.1.b	Po	0	841	0.91	88.4	17.1	11.0	0.92
B.4.a	Po	25 cm	710	0.92	185.9	24.8	24.8	1.04
B.4.b	Po	25 cm	841	1.12	235.3	31.5	24.9	1.24

If measuring the inference accuracy in terms of rRMSE on Q, the results obtained for these 12 experiments show that rough priors $Q^{(0)}$ (see paragraph 4.3) may lead to poor estimations of the discharge, see Table 5. For the A.1.a case $rRMSE_Q = 4.8\,\%$ which is really better than for the A.1.b case where $rRMSE_Q = 30.5\,\%$. For the A.4.a case $rRMSE_Q = 9.0\,\%$ and $rRMSE_Q = 33.0\,\%$ for the A.4.b case. The same observation can be made for the Po River.

However, as shown in Figure 2, the infered temporal variations of Q remain excellent in all cases. Indeed, if we compute the same rRMSE but using $Q^*(x,t) = \frac{\bar{Q}_{true}}{\bar{Q}^{(0)}} Q(x,t)$ (i.e. the shift of the prior is taken into account) the obtained values are: $rRMSE_{Q*} = 7.6\,\%$ for the A.1.b case, $rRMSE_{Q*} = 13.3\,\%$ for the A.4.b case, $rRMSE_{Q*} = 11.0\,\%$ for the B.1.b case and $rRMSE_{Q*} = 24.9\,\%$ for the B.4.b case. Thus the rRMSE obtained are comparable with the rRMSE obtained using the good prior. This high accuracy of the discharge temporal variation independently of the priori quality is mathematically explained in the next paragraph 5.3.

In other respects, these results show that the estimations are highly sensitive to the accuracy of the inflow prior if using the simple *"Manning"* method. On the contrary, if using multiple accurate discharges values (here from the GRDC database) that is using the *"Manning-Multi"* method, these estimations are much more robust.

5.3 On the equifinality issue & the importance of one ancillary data

The numerical results above show that the discharge inference may be very accurate if the (scalar) prior value $Q^{(0)}$ is relatively accurate; it may be the mean value of Q. On the contrary if the priori value(s), see paragraph 4.3, are far from reality, the rRMSE on the estimated $Q(t)$ may be large, see e.g. case A.4.b in Tab. 4. However it has been noticed above by evaluating the rRMSE from $Q^*(x,t)$ that even in such a case the infered temporal variations of Q are excellent (see Fig. 2). This equifinality issue can be explained by re-scaling the flow equations as follows.

Let $\bar{Q}$ be a scalar value e.g. a mean value of Q or even K. The variables (A, Q, h) are re-scaled as follows: $(A_*, Q_*, h_*) = (A, Q, h)/\bar{Q}$. We set: $A_* = h_* W$; W the measured surface width. The mass equation divided by $\bar{Q}$ reads: $\partial_t(A_*) + \partial_x(Q_*) = 0$. Therefore as it is well known, in terms of mass, rescaling Q implies to rescale A by the

same factor (or equivalently rescaling the water depth h). The momentum equation divided by $\bar{Q}$ reads:

$$\partial_t(Q_*) + \partial_x\left(\frac{Q_*^2}{A_*}\right) + gA_*\,\partial_x Z = -gA_*S_f$$

with $S_f \equiv S_f(A,Q;h;K) = \frac{1}{K^2}\frac{|Q|Q}{A^2h^{4/3}}$. A short calculation shows that: $S_f(A,Q,h;K) = S_f(A_*,Q_*,h_*;\bar{K}^{-2/3}K)$. Therefore, *given the WS* measurements (W,Z), the 1D Saint-Venant equations (1) with K as Manning-Strickler's coefficient is equivalent to the same equation but in the re-scaled variables (A_*,Q_*,h_*) and with $(\bar{K}^{-2/3}K)$ as Manning-Strickler's coefficient. As a consequence the infered solution $(A,Q;K)$ obtained by inverting the Saint-Venant model is those corresponding to the prior value(s) introduced into the vector c_{prior}, see (9) and Section 4.3. (Recall that the first guess value $Q^{(0)}$ and the values considered at downstream for the rating curve conditions are consistent).

The mathematical development above and the numerical results based on WS measurements only show that the VDA process is actually accurate to retrieve the temporal variations of the discharge $Q(t)$ but it may be to a multiplicative factor. On the contrary, as demonstrated in the next section, this equifinality issue is solved as soon as a reference value of one of the three fields A_0 (or equivalently b), Q or K is provided. A global mean value may be enough thanks to the low complexity system (13) solved to obtain the first guess values, see Section 4.3.

It is worth noticing that inversions based on low complexity models, the Manning-Strickler equation or the low complexity system (4), present equifinality issue even stiffer. Indeed, given a set of WS measurements $(Z_{r,p},W_{r,p})_{R,P+1}$ and an effective low flow bathymetry $A_{0,r}\,\forall r$ (therefore the effective cross-sectional area $A_{r,p} = A_{r,0} + \delta A_{r,p}\ \forall r \in [1..R]$ is given), the inference of the *ratio* $Q_{r,p}/K_{r,p}$ is possible from 4 but not the pair $(Q_{r,p},K_{r,p})$. Infering the discharge value from the WS measurements and local Manning-Strickler's laws i.e. the low Froude system (4), requires additional information on the roughness coefficient. Otherwise the resulting uncertainty on Q is proportional to the uncertainty on K^{-1}, and reciprocally. Of course, given a strong prior information on Kor Q i.e. an a-priori pdf, the corresponding uncertainty on the infered value may be computed.

5.4 Identifiability map (Sacramento River)

The discharge inference capabilities depend on the space-time sampling of the observations and on the flow dynamics. An instructive reading of the inverse problem stiffness can be obtained by plotting the "identifiability map" introduced in Brisset et al., 2018. The identifiability map represents in the (x,t) plane the complete information : the "space-time windows" observed by SWOT, the hydrodynamic wave propagation (1D Saint-Venant model in fluvial regime) and the misfit to the "local equilibrium" (local misfit between the steady state uniform flow and the dynamics flow), see Brisset et al., 2018 for more details. This preliminary analysis enables to roughly estimate the inflow time intervals that can be quantified by VDA (the inflow discharge values arise from these observed "space-time windows"). This quantitative reading of the inverse problem is instructive since it enables to roughly estimate if the sought information has been observed or not. In the present case (Sacramento River case), the reach of 147 km long is completely observed by two SWOT tracks respectively at day 9 and 19 for each 21 days repeat period.

As the Sacramento River is considered ungauged in this experiment, the real identifiability map cannot be computed. To circumvent this we compute an *a-priori* identifiability map using the following method:

- First we perform a VDA inference of the control vector c using prior information given by the "*Manning*" method (Section 4.1) and SWOT observables.
- Then, using the obtained control vector c we compute a forward run using the full Saint-Venant model (1).
- Finally, the "equilibrium misfit" $(S_f - S_0)$ and the wave propagation times (T_{wave}) are calculated using the output of the forward model.

The obtained identifiability map is plotted on Fig. 3. Due to the observation layover there are few unobserved zones for the second SWOT pass #527, for example at $x = 80$ km and $t = 19, 40, 61$ days. Given the WS observation of each reach at a given time, on Fig. 3 purple dots at the upstream BC represent the foot of each hydraulic characteristics - the upward hydraulic information propagation. Then, the identifiability of $Q_{in}(t)$ appears to be possible on time windows of $\sim$3 days ($\sim$2 days for the flood peak recession at day 51) before observation times.

Another information, the "equilibrium misfit", is represented on this map and it highlights where and when the flow is not locally steady and uniform. The magnitude of this equilibrium misfit tends to increase when a flood wave is traveling through the domain as shown by the observation at day 51, and day 61 corresponding to another peak entering the studied domain, Fig. 3 and 4. The map indicates that the WS deformations due to the flood peak between day 51 and 61 have not been observed. Moreover the mean estimated upward information propagation time is of 72h.

Consequently, from this analysis we define 3 assimilation points every 12h, hence corresponding to half the mean propagation time, before observations at days 51 and 61. Those observations may contain information respectively on the first flood peak recession and the third flood peak rise. The mean estimated upward propagation time is 36h (estimation coming from "observable times", which are represented with vertical purple dots on the right side of the figure). Since these "observable times" are computed a-posteriori and using an estimation of the wave speeds, we dismissed the extrema values (we retain 70% of the values).

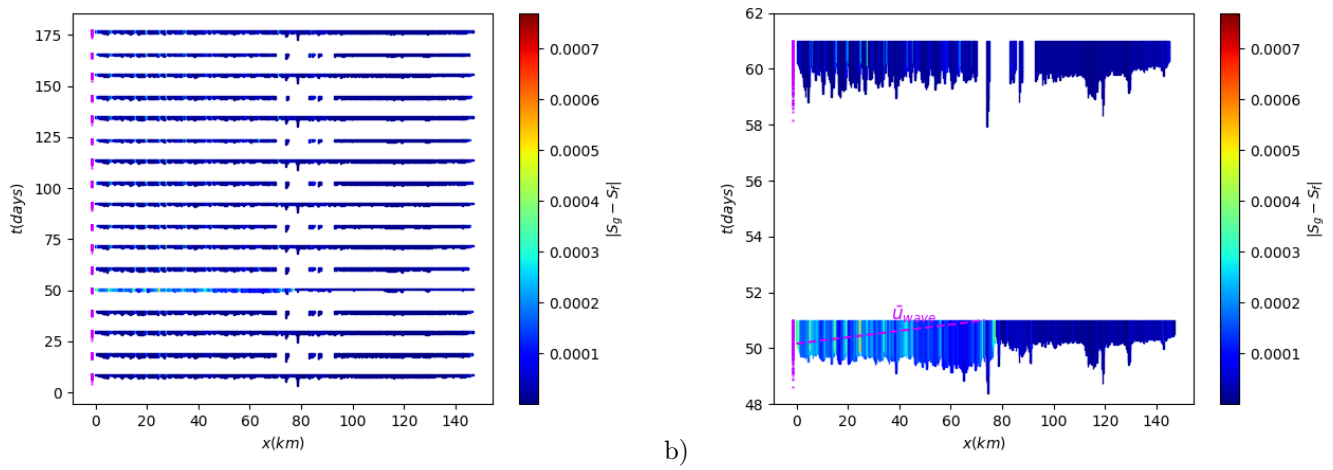

a) b)

Figure 3: Identifiability map: overview in the (x,t)-plane of the inverse problem features: observables, hydraulic wave speed (and "equilibrium misfit" being absolute value of the source term in the Saint-Venant equations, color bar). For each observation of the domain in time, the vertical spreading corresponds to the time $\frac{\alpha}{u}\Delta x$ necessary for the upstream wave to cross an observed cell of size Δx; α is simply a dilatation factor for a sake of readability. . (a) The complete (x,t)-plane. (b) Zoom on the most varying time interval.

5.5 SWOT scenario: Sacramento River

The accuracy and the robustness of the algorithms proposed in this study are demonstrated on a real SWOT scenario, that is with relatively sparse observations in time compared to the inflow hydrograph frequencies. The identifiability maps provide some crucial information to define assimilation points before SWOT observation points. Indeed WS deformations observed at a given time over a river domain are caused by past variations of the sought inflow hydrograph at the upstream of the river domain. The inflow discharge, bathymetry and roughness infered by VDA on the Sacramento River are shown respectively on Fig. 4 (a) and Table 5. As expected following the analysis made above with identifiability maps, the discharge identification is accurate at each observation time and for the 3 points preceding observed flood peaks at $t = 51$ and 61 days. It is worth noticing that a basic approach consisting in infering discharge at observation times only would lead to a less accurate hydrograph inference as shown in Fig. 4 (b). Recall that the flood peak between days 51 and 61 is not retrieved since the analysis above shows that the peak effects have not been observed.

Following Brisset et al., 2018, the identifiability index $I_{ident} = \frac{T_{wave}}{\Delta t_{obs}}$ of the river case is evaluated for a wave propagation time (T_{wave}) of about $72h$ (with $\Delta t_{obs} \sim 10$ days), it gives $I_{ident} \sim 0.3$, that is a relatively low identifiability index. Interestingly, even with this low identifiability value, the inference of discharge is accurate at observation points but also at the identification times defined before flood observations thanks to identifiability maps. This demonstrates the value of using such *a-priori* reading of the inverse problem enabling the definition of identification times before observations.

Finally we point out that the infered discharge is accurate while the bathymetry and roughness need to be refined using other information or equations; this is done in next section using the low complexity relations presented in Section 2.3. In other respect, this test case highlights the importance of using a complete unsteady flow model to simulate non-linear dynamics between the sparse assimilation points.

6 Inferences from WS observations and one in-situ measurement

Fortunately many worldwide rivers are not (fully) ungauged. In this section the benefit of using additional ancillary data is investigated. A bathymetry measurement can be valued with the Low Froude model (Eqn 5) allowing the estimate of an accurate bathymetry first guess of the control vector $c^{(0)}$ in the VDA process (case *"Low Froude"* Section 4.3). Next, an approach based on Manning equation is developed below to take advantage of discharge data if available, provided for example by a hydrological model or a gauging station, for estimating a first guess of the full control vector (case *"Manning-multi"* Section 4.3).

On the accuracy of these low Froude - low complexity systems (4) and (5). As already mentioned, the low Froude - low complexity systems (4) and (5) have been numerically assessed into detail for the present test rivers. For the Po and Garonne rivers, the HEC-RAS model (US Department of Defense, Army Corps of Engineers) have been used

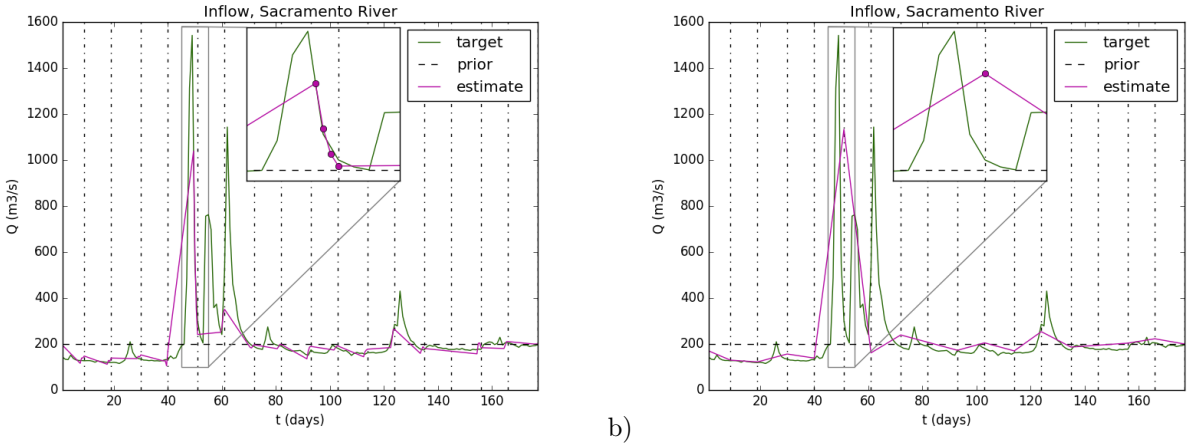

a) b)

Figure 4: Inflow discharge (target=true, prior and infered=estimate with SWOT-HR observations), Sacramento River. Computations with $N = 4$ assimilation points every ($0h$,$12h$,$24h$,$36h$) before observation times (a) or at observation times only (b).

to generate synthetic observations; next Gaussian noises with realistic variances are added, see Section 4.1. For the Sacramento river, SWOT Hydrology Simulator outputs have been considered. Then these direct runs provide the considered "true" flows measurements. Next given the effective true bathymetry b and the synthetic data $(Z, WS^{1/2})$, the Manning-Strickler system (4) is solved and its solution is compared to the "true" one. The obtained difference between the discharge values deduced from (4) and the "true" values equals approximatively $\pm 7\%$, see Fig. 7.

The obtained difference between the unobserved flow area A_0 infered from (5) and W_0, and the effective "true" value equals approximatively $\pm 10\%$ in ≈ 100 km long reaches, see Fig. 6.

It is worth noting that this estimation presents an increasing "drift" from the reference in-situ measurement location x_{ref}. As discussed in Garambois and Monnier (2015), this drift is due to the non consistency of the steady state mass conservation $\partial_x Q = 0$. However this low Froude bathymetry is accurate enough if applied to a ~ 100 km portion only (for a single measurement h_{ref}) (recall that neither tributary flows nor groundwater exchanges are taken into account in the present modeling).

6.1 Inference of A_0 from one in-situ bathymetry measurement

As already pointed out, infering the pair $(Q(t); K)$ given the bathymetry b is much less challenging; this is one of the context analyzed in detail in Brisset et al. (2018). Therefore infering a reliable prior bathymetry before the iterative VDA process may be highly interesting. Here the control vector c, see (6), is composed by the upstream discharge, the bathymetry and the roughness. In this paragraph the different alternatives presented in Section 4.3 for estimating low flow bathymetry are tested on the three rivers, see Fig. 5. Each method gives fairly good estimations of $(b_r)_{1..R}$ (represented here as B^* the bed elevation b minus an average bathymetry trend). For each river, unsurprisingly, the best estimate is given by the low Froude approach, Eqn (5) requiring one in-situ point. Using the approaches based on the Manning equation and one flow line ($b^{(0)}$ *"Manning"*, Eqn (4)) leads to a shift of the infered prior bathymetry (Po and Sacramento rivers) whereas it is avoided if using the low complexity approach involving multiple flow lines better sampling flow regimes ($b^{(0)}$ *"Manning-multi"*, Eqn (13)).

In the Sacramento river case, a drift (increasing error in space) appears in the *"Low Froude"* bathymetry for nodes far from the reference point. Indeed if the basic hypothesis $\partial_x Q = 0$ of *"Low Froude"* model is not satisfied (that is an unsteady flow), such a drift appears due to the nature of the differential equation (a first order differential equation), see Garambois and Monnier, 2015 for a detailed investigation. In order to avoid this drift, a segmentation of the river into two zones is performed and two reference bathymetry points are used for the *"Low Froude"* bathymetry prior estimation, Fig. 5 (Bottom Right).

6.2 Inference of (A_0, K) from one gauging station

This section presents a low complexity model derived for taking advantage of spatio-temporal discharge data if available, for example provided by a regional scale hydrological model or a gauging station close from the studied zone and applied to each reach. In other words, let us assume that spatially distributed values of Q are available on the river portion for each overpass $p \in [0...P]$, that is $(Q_{r,p})_{r,p}$. These values may be provided by a hydrological model or computed by the VDA algorithm presented in Section 3. Let us assume that the roughness varies both in space and time, that is $(K_{r,p})_{r,p}$. Then (4) reads as follows:

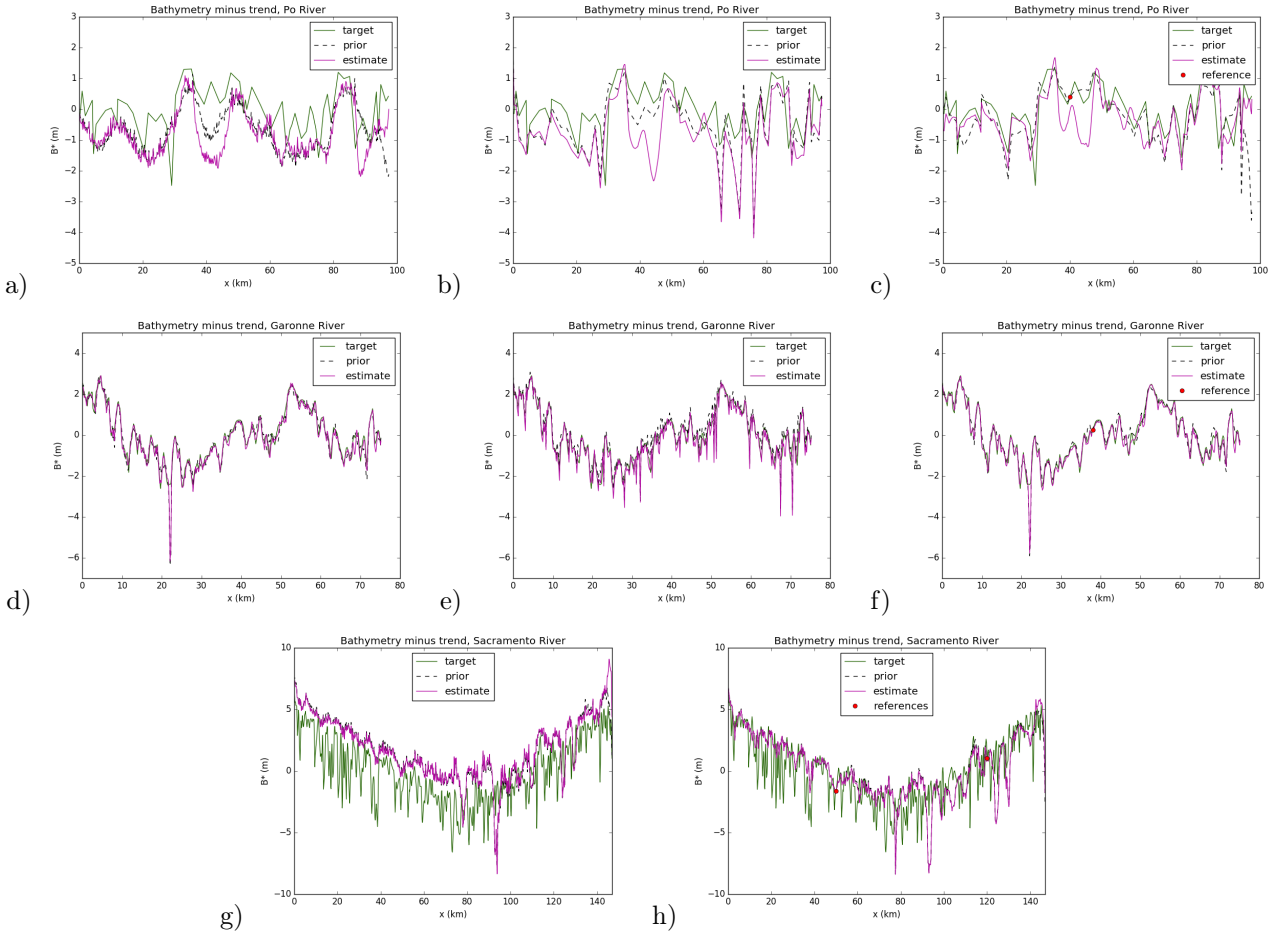

Figure 5: True and infered bathymetry deviation from trend $(B^*)_{1..R}$ compared to prior bathymetry estimations, noisy observations (Section 4.3): (a,d,g) "Manning". (b,e) "Manning-multi". (c,f,h) "Low Froude".

$$c_{r,p} \cdot K_{r,p}^{3/5} A_{r,0} + d_{r,p} \cdot K_{r,p}^{3/5} = Q_{r,p}^{3/5} \text{ for all } (r,p) \tag{13}$$

with $c_{r,p} = W_{r,p}^{-2/5} S_{r,p}^{3/10}$ and $d_{r,p} = c_{r,p}\, \delta A_{r,p}$. The coefficients $(c_{r,p}\ , d_{r,p})$ can be evaluated from the altimetry measurements. System (13) is multi-linear in $(K_{r,p}^{3/5} A_{r,0}, K_{r,p}^{3/5}, \bar{Q}_p)$. It contains $R(P+1)$ equations. It can be employed differently depending on the available information and the unknowns. If considering the full set of unknowns $(K_{r,p}^{3/5}, A_{r,0}, Q_{r,p})$, it is an underdetermined system since it has $R(2(P+1)+1)$ unknowns; therefore in this case it cannot be solved since it has an infinity of solutions.

Let us define the diagonal matrices D_c and D_d of dimensions $[R(P+1)]^2$ by: $M_c = diag\,(c_{r,p})$, $M_d = diag\,(d_{r,p})$. Let us define the vectors : $\tilde{K} = (K_{r,p}^{3/5})_{r,p} \in R^{R(P+1)}$, $A = (A_{r,0})_r, \in R^R$ and $\tilde{Q} = (Q_{r,p}^{3/5})_{r,p} \in R^{R(P+1)}$. Then (13) reads:

$$D_c\, Bil(\tilde{K}, A) + D_d \tilde{K} = \tilde{Q} \text{ in } R^{R(P+1)} \tag{14}$$

with the bilinear operator $Bil(\tilde{K}, A)_{r,p} = K_{r,p}^{3/5} A_{r,0}\ \forall r \forall p$. If $\tilde{Q}$ is given then (14) has $(P+2)R$ unknowns (the two vectors $\tilde{K}$ and A).

For K constant in space but varying in time (e.g. K is defined as a power law in h) then $\tilde{K} = (K_p^{3/5})_p \in R^{(P+1)}$. In this case, the $(P+1+R)$ unknowns $(K_p^{3/5}, A_{r,0})$ can be computed by solving the overdetermined bi-linear system (14) e.g. by employing a trusted region reflective algorithm.

For K constant in time but varying in space, $\tilde{K} = (K_r^{3/5})_r \in R^R$, the system (14) has $2R$ unknowns. Therefore if $P \geq 1$ (more than 2 overpasses), the solution $(K_r^{3/5}, A_{r,0})$ can be computed e.g. by a trusted region reflective algorithm.

Then the RHS of (14) reads: $\bar{Q} = \left((\bar{Q}_0^{3/5}, ..., \bar{Q}_0^{3/5}), ..., (\bar{Q}_p^{3/5} ... \bar{Q}_p^{3/5}), ..., (\bar{Q}_P^{3/5} ... \bar{Q}_P^{3/5})\right) \in R^{R(P+1)}$. Given $\bar{Q}$, estimations of $(A_{r,0})_r$ are obtained by computing the pairs $(K_{r,p}, A_{r,0})_{r,p}$ solution of (14) (with the values of $(K_{r,p})$ not necessarily used).

In some contexts one can have prior estimations of $Q = (Q_{r,p}) \in R^{R(P+1)}$ provided by a hydrological model for instance, see e.g. Wisser et al. (2010); Paiva et al. (2011); Schellekens et al. (2017); then (14) can be solved to obtain effective unobserved wetted areas $(A_{r,0})_r$.

6.3 Inferences of $(Q(t), b(x), K)$ by VDA using one in-situ measurement

In this paragraph, the impact of bathymetry prior on the control vector c (see Eqn (6)) infered by VDA is detailed. For each river, the infered inflow hydrograph starting from a "Low Froude bathymetry" prior (see Section 6.1 and Fig. 5) is shown on Fig. 6.

For the Sacramento river, both VDA runs C.3 and C.4, performed either with *"Manning"* or *"Low Froude"* bathymetry priors, result in comparable errors ($rRMSE_Q \sim 20\%$). The bathymetry is slightly degraded but the inversion remains robust.

For the Garonne River the inversions performed with the 3 different bathymetry first guesses result in comparable errors ($rRMSE_Q = 8.5\%$ and 9.1%, runs C.3 and C.4). The finest bathymetry infered by VDA results from the use of *"Manning"* or *"Low Froude"* bathymetry first guesses - that provide fairly accurate priors in that case.

For the Po River, using a *"Low Froude"* bathymetry results in the best error ($rRMSE_Q = 18.3\%$, run B.6) compared to other bathymetry first guesses (runs B.4 and B.5). This bathymetry is also slightly improved by the VDA process.

As shown in Section 5.2 the accuracy of the infered triplet $(Q(t), b(x), K)$ with the present algorithms depend on the accuracy of the prior estimations; however due to the change of variable and covariance operators introduced in the VDA formulation (making the "regularization" of the inverse problem, see Section 3), the triplet inference is robust (in terms of convergence and computed optimal solution).

7 Real-time estimations of Q given (A_0, K)

As previously shown, robust and accurate estimations of the discharge may be obtained using the present inversion algorithms (VDA process, prior strategies and Saint-Venant equations) and SWOT observations set. It is highly advisable to perform theses inversions on a complete hydrological cycle (i.e. a complete hydrological year) since the VDA process provides optimal values in a least-square sense with respect to the observations sampling. However it is important to recall that K (constant or not) is model dependent; moreover the iterative VDA process cannot be performed in real-time (because of latency of satellite data after aquirement) yet.

Therefore once the VDA based inversion process has been performed on a complete SWOT observation set (that is the so-called calibration or learning period), quite accurate values of $(A_{r,0}) \in R^R$ and $(Q_{r,p}) \in R^{R(P+1)}$ are available. Next the discrete low Froude / low complexity system (4) is quite accurate, see e.g. Fig. 7 and can be solved in

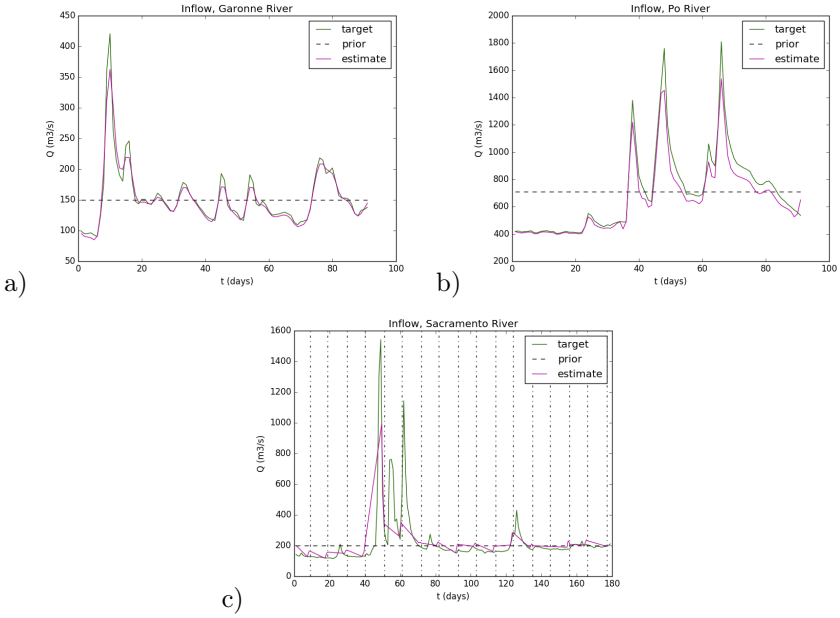

Figure 6: infered inflow discharge with the bathymetry priors infered using the Low-Froude model and one (1) in-situ point ($b^{(0)}$ "Low Froude"). Daily SWOT-like observations (noise $\sigma_Z = 0.25$) (a, b) and SWOT-HR observations (c).

Table 5: Scores of the inversions performed from different priors defining the bathymetry first guess $b^{(0)}$, see Section 4.3.

Case	River	σ_Z^{obs}	b_{prior}	$RMSE_{b^{(0)}}$ (m)	$RMSE_Q$ (m^3/s)	$rRMSE_Q$ (%)	$RMSE_b$ (m)
A.1	Garonne	0	Manning	0.18	13.4	5.1	0.27
A.2	Garonne	0	Manning-multi	0.17	10.0	4.2	0.16
A.3	Garonne	0	Low Froude	0.16	11.9	5.2	0.22
A.4	Garonne	25 cm	Manning	0.39	24.0	10.3	0.31
A.5	Garonne	25 cm	Manning-multi	0.42	17.9	8.5	0.38
A.6	Garonne	25 cm	Low Froude	0.35	19.4	9.1	0.27
B.1	Po	0	Manning	0.61	83.9	8.5	0.75
B.2	Po	0	Manning-multi	0.73	91.2	10.2	0.88
B.3	Po	0	Low Froude	0.48	76.4	7.8	0.45
B.4	Po	25 cm	Manning	0.92	185.9	24.8	1.04
B.5	Po	25 cm	Manning-multi	0.83	183.7	24.3	1.07
B.6	Po	25 cm	Low Froude	0.64	144.8	18.3	0.60
C.1	Sacramento	0	Manning	2.29	30.1	11.5	2.33
C.2	Sacramento	0	Low Froude	1.95	54.5	15.9	2.01
C.3	Sacramento	34 cm	Manning	2.45	124.7	19.3	2.49
C.4	Sacramento	34 cm	Low Froude	1.84	141.2	20.2	1.82

real-time. Then given $(Q_{r,p}, A_{r,0})_{r,p}$ by the VDA algorithm, the effective space-time dependent roughness coefficient $(K_{r,p})_{r,p}$ is computed from (14). Next given new observations sets $(Z_r, W_r)_R$, typically satellite observations acquired after the "learning period", the corresponding discharge values Q_r can be computed in real-time simply by evaluating the Manning-Strickler equation (4). Such real-time estimations are presented in Section 7.

7.1 Roughness coefficient re-calibration

The roughness roughly estimated by VDA due to the equifinality problem detailed above can be re-calibrated; hence enabling to infer the discharge in real-time with a simple flow model (i.e. as soon as new SWOT measurements are acquired).

The re-calibration of the roughness coefficient is done following one of these two methods:

- $K_r = mean_p(K_{r,p})$, hence K is constant in time by time intervals. The mean is computed on a subset of the WS observations e.g. by considering the 2^{nd} - 8^{th} deciles of the flow profiles (here 20 overpasses) since this corresponds to a relatively wide and representative range of flow regimes without the extremes. We compute $K_{r,p}$ by inverting Eqn (4); next the temporal averaging above provides the spatially distributed roughness coefficient K_r.
- $K_{r,p} = K_r(h_{r,p}) = \alpha_r {h_{r,p}}^{\beta_r}$, with α_r and β_r defined for each river reach, hence distributed in time and space. It is estimated from the low flow bathymetry $(b_r)_{1..R}$ infered by VDA, hence providing the water depth $h_{r,p}$. Note that the hydraulic parameters are infered on the 1D model grid which is finer than the observation grid, hence the inversion outputs are aggregated (spatial average) on each reach r, $r \in [1..R]$. Next, $h_{r,p} = (Z_{r,p} - b_r)$, and for each reach r a simple least-square fitting with respect to (α_r, β_r) provides $K_{r,p} = \alpha_r {h_{r,p}}^{\beta_r}$.

These two methods are adequate in our cases since no over-bank flow occurs; they are applied to the Garonne and Po rivers only. These are not applied to Sacramento River since the number of observations was not sufficient to select reliable 2^{nd} - 8^{th} deciles of the flow profiles.

7.2 Real-time estimations of Q

Given the re-calibrated roughness coefficients $(K_r)_{1..R}$ above, the discharge is computed using simply the Manning-Strickler equation (4) from the newly acquired SWOT like observations. The obtained values in the case of the Po and Garonne Rivers are plotted on Fig. 7 for all available flow lines. (Note that WS slopes are obtained by downstream finite difference from observed WS elevation between two observed points).

For both rivers, using a roughness coefficient K_r constant in time gives the best results. The resulting errors are: $rRMSE_Q = 6.3\%$ for the Garonne River and $rRMSE_Q = 10.6\%$ for the Po River. Note that these performances are evaluated at all observation times and all nodes whereas for the VDA inference (Section 5) the performances are evaluated only for the upstream node of the river domain, i.e. only for $r = 0$.

The second method for re-calibrating the roughness $K_{r,p}$ provides low accuracy but still good; the errors are: $rRMSE_Q = 9.1\%$ for the Garonne River and $rRMSE_Q = 25.3\%$ for the Po River.

Recall that the flow model is calibrated from the observed regimes hence presenting a minimal and a maximal WS elevation. The re-calibrated roughness coefficient K is related to this flow regime range. If K is defined as a power-law $K_{r,p}$ and if the newly acquired WS elevation is greater than the previously observed WS than the roughness power-law is prone to an over-estimation. That is the reason why we encourage to use the first method (i.e. by considering K_r and not the power-law).

Finally the proposed approach based on the low complexity systems (employed after a re-calibration of the roughness coefficient as presented above) appears very promising to perform the discharge in real-time, that is in an operational way.

8 Conclusion

This study proposes a new computational hierarchical strategy to infer the discharge $Q(t)$, an effective bathymetry $b(x)$ plus a corresponding roughness coefficient K from WS altimetry data; more specifically the forthcoming SWOT satellite measurements. The inverse algorithm is based on a combination of an advanced Variational Data Assimilation (VDA) formulation applied to the Saint-Venant equations (1D shallow-water) and original low complexity algebraic systems (low-Froude flow laws, locally permanent). The VDA formulation takes into account a-priori scale dependency and a-priori error measurement amplitudes. The cross sections are effective since they are defined from the satellite measurements (trapezium super-impositions). Three rivers, ~ 100 km long each, have been considered with two scenarios of observation: the SWOT Cal-Val orbit with ~ 1 day period (or any equivalent multiple-sensor measurements) and SWOT like data with ~ 21 days period (with 1 to 4 passes at mid-latitudes). The corresponding inversions are highly challenging since relying on relatively sparse observations (both in space and time) compared to the potential flow dynamics (the flows present low identifiability indexes as defined in Brisset et al., 2018). Preliminary analysis

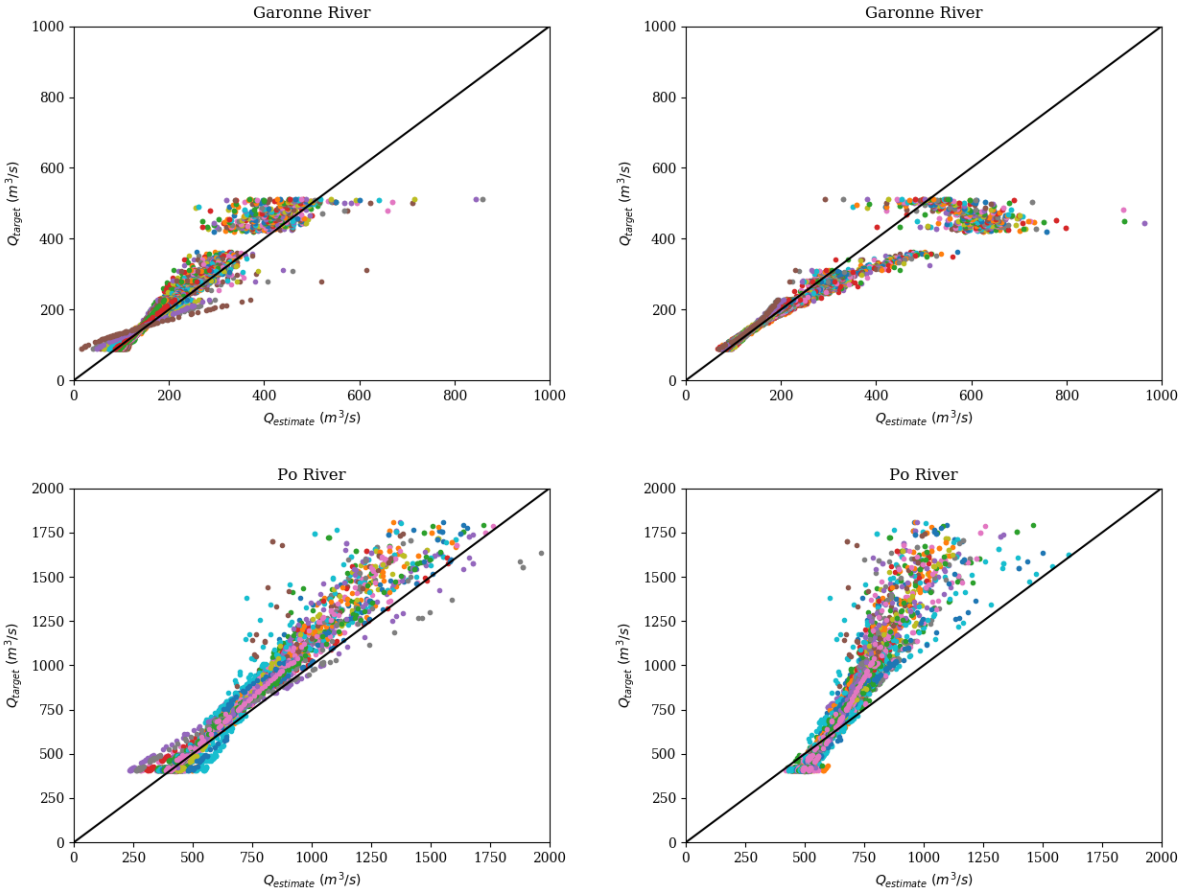

Figure 7: Discharge computations from the low complexity relations obtained after the re-calibration of the roughness K obtained by the VDA process; Plot Q_{true} vs $Q_{infered}$ using (4) on the complete observations set. (Top). Discharge Garonne River; (Bottom) Po River. (Left) With $K(h)$ hence K_p; (Right) With K_r.

based on the identifiability maps introduced in Brisset et al., 2018 help to define adequate time grids for the VDA identification process.

The key ingredients of these original inversions are the advanced VDA formulation, a relatively complete dynamic model (the Saint-Venant equations) but also the original low Froude - low complexity systems which have been especially derived for the present context. These low complexity algebraic systems enable to exploit in a physically consistent manner databases to define first guesses (prior information) of the iterative VDA process. Moreover they enable to compute in real-time the discharge past the "calibration period" by the VDA process i.e. past the assimilation of a complete hydrological year.

For ungauged rivers and/or in total absence of good prior information on the flow, the inversion algorithm provides accurate temporal variations of $Q(t)$ with an effective bathymetry $b(x)$ and a corresponding roughness coefficient $K(h)$ (K function of the water depth h) around the first guess mean values. The VDA process applied to the hydrodynamic model propagates remarkably in space-time the informative content of the WS measurements. However if the prior mean value (e.g. of Q) is far from reality, a multiplicative factor of the infered hydrograph $Q(t)$ may remain. On the contrary, as soon as a good mean value is provided, e.g. a mean discharge value from a database or a large scale hydrological model or a single reference value of bathymetry, thanks to the resolution of the low complexity system before the VDA process, the equifinality issue is removed: the discharge $Q(t)$ is perfectly recovered (RMSE of a few percent at observation times). Past the calibration period by VDA (e.g. one year), the estimated values of $Q(t)$ and $b(x)$ obtained by the VDA process are employed to re-calibrate the roughness coefficient $K(x)$ corresponding to the low-complexity model. Next, this low complexity model provides estimations of the discharge Q *in real-time* from the newly acquired satellite data. All the present equations and algorithms are implemented into the open-source computational software DassFlow (DassFlow, 2018). On-going investigations focus on inversions applied to larger rivers presenting lateral fluxes and complete river networks.

Authors' contributions & acknowledgments

The first author has largely enriched the computational software DassFlow1D from the previous version developed by P. Brisset (Brisset et al., 2018) and has performed the numerical results. The second author has elaborated the hierarchical modeling approach, the equations and the main algorithms. The third author has greatly contributed to the real data model setups, their analysis and suggested the sensitivity to first guess and densified temporal identifiability. The last author has nicely contributed to the understanding of the advanced VDA formulation (beginning of his PhD). All the authors have merged their knowledge all along the research to finally obtain the present result.

The authors K. Larnier (software engineer at CS corp.) and J. Verley (software engineer during 10 months next PhD student IMT-INSA-CLS 17-18) have been funded by CNES. The two other authors have been partly supported by CNES TOSCA research project 14-18. The authors acknowledge M. Durand from Ohio State University for providing the Sacramento SWOT-HR dataset; also H. Roux from IMFT and INPT-Toulouse University has provided a fine expertise on the Garonne River dataset.

References

G. H. Allen and T. M. Pavelsky. Patterns of river width and surface area revealed by the satellite-derived north american river width data set. *Geophysical Research Letters*, 42(2):395–402, 2015. ISSN 1944-8007. doi: 10.1002/2014GL062764.

George H. Allen and Tamlin M. Pavelsky. Global extent of rivers and streams. *Science*, 361(6402):585–588, 2018. ISSN 0036-8075. doi: 10.1126/science.aat0636. URL `http://science.sciencemag.org/content/361/6402/585`.

K. Andreadis, G. Schumann, and T. Pavelsky. A simple global river bankfull width and depth database. *Water Resources Research*, 49(10):7164–7168, 2013. ISSN 1944-7973. doi: 10.1002/wrcr.20440. URL `http://dx.doi.org/10.1002/wrcr.20440`.

G. Aronica, B. Hankin, and K. Beven. Uncertainty and equifinality in calibrating distributed roughness coefficients in a flood propagation model with limited data. *Advances in Water Resources*, 22 (4):349 – 365, 1998. ISSN 0309-1708. doi: https://doi.org/10.1016/S0309-1708(98)00017-7. URL `http://www.sciencedirect.com/science/article/pii/S0309170898000177`.

E. Bélanger and A. Vincent. Data assimilation (4d-var) to forecast flood in shallow-waters with sediment erosion. *Journal of Hydrology*, 300(14):114 – 125, 2005. ISSN 0022-1694. doi: http://dx.doi.org/10.1016/j.jhydrol.2004.06.009. URL `http://www.sciencedirect.com/science/article/pii/S0022169404002914`.

S. Biancamaria, K. M. Andreadis, M. Durand, E. A. Clark, E. Rodriguez, N. M. Mognard, D. E. Alsdorf, D. P. Lettenmaier, and Y. Oudin. Preliminary characterization of SWOT hydrology error budget and global capabilities. *Selected Topics in Applied Earth Observations and Remote Sensing, IEEE Journal of*, 3:6–19, 2010. 1.

S. Biancamaria, M. Durand, K.M. Andreadis, P.D. Bates, A. Boone, N.M. Mognard, E. Rodriguez, D.E. Alsdorf, D.P. Lettenmaier, and E.A. Clark. Assimilation of virtual wide swath altimetry to improve arctic river modeling. *Remote Sensing of Environment*, 115(2):373 – 381, 2011. ISSN 0034-4257. doi: https://doi.org/10.1016/j.rse.2010.09.008. URL http://www.sciencedirect.com/science/article/pii/S0034425710002816.

S. Biancamaria, D. P. Lettenmaier, and T. M. Pavelsky. The swot mission and its capabilities for land hydrology. *Surveys in Geophysics*, 37(2):307–337, Mar 2016. ISSN 1573-0956. doi: 10.1007/s10712-015-9346-y. URL http://dx.doi.org/10.1007/s10712-015-9346-y.

D. M. Bjerklie. Estimating the bankfull velocity and discharge for rivers using remotely sensed river morphology information. *Journal of hydrology*, 341(3):144–155, 2007.

David M. Bjerklie, S. Lawrence Dingman, and Carl H. Bolster. Comparison of constitutive flow resistance equations based on the manning and chezy equations applied to natural rivers. *Water Resources Research*, 41(11), 2005. doi: 10.1029/2004WR003776. URL https://agupubs.onlinelibrary.wiley.com/doi/abs/10.1029/2004WR003776.

David M. Bjerklie, Charon M. Birkett, John W. Jones, Claudia Carabajal, Jennifer A. Rover, John W. Fulton, and Garambois P-A. Satellite remote sensing estimation of river discharge: Application to the yukon river alaska. *Journal of Hydrology*, 561:1000 – 1018, 2018. ISSN 0022-1694. doi: https://doi.org/10.1016/j.jhydrol.2018.04.005. URL http://www.sciencedirect.com/science/article/pii/S0022169418302464.

F Bouttier and P Courtier. Data assimilation concepts and methods march 1999. *Meteorological training course lecture series. ECMWF*, page 59, 2002.

P. Brisset, J. Monnier, P.-A. Garambois, and H. Roux. On the assimilation of altimetric data in 1d saint-venant river flow models. *Adv. Water Ress.*, 119:41–59, 2018.

DG Cacuci, IM. Navon, and M. Ionescu-Bugor. *Computational Methods for Data Evaluation and Assimilation*. Taylor and Francis CRC Press: Boca Raton, 2013.

S. Calmant, J.-F. Cretaux, and F. Remy. 4 - principles of radar satellite altimetry for application on inland waters. In Nicolas Baghdadi and Mehrez Zribi, editors, *Microwave Remote Sensing of Land Surface*, pages 175 – 218. Elsevier, 2016. ISBN 978-1-78548-159-8. doi: https://doi.org/10.1016/B978-1-78548-159-8.50004-9. URL https://www.sciencedirect.com/science/article/pii/B9781785481598500049.

M. Carlier. *Hydraulique générale et appliquée*. Eyrolles, Paris, France, 1982.

W. Castaings, D. Dartus, M. Honnorat, F.-X. Le Dimet, Y. Loukili, and J. Monnier. Automatic differentiation: a tool for variational data assimilation and adjoint sensitivity analysis for flood modeling. In *Automatic Differentiation: Applications, Theory, and Implementations*, pages 249–262. Springer, 2006.

DL Chertok and RW Lardner. Variational data assimilation for a nonlinear hydraulic model. *Applied mathematical modelling*, 20(9):675–682, 1996.

V.T. Chow. *Open-channel Hydraulics*. Mc Graw-Hill, New-York, USA, 1959.

V.T. Chow. Handbook of applied hydrology. *McGraw-Hill Book Co., New-York, 1467 pages*, 1964.

S. Cohen, A. Kettner, and J. Syvitski. Global suspended sediment and water discharge dynamics between 1960 and 2010: Continental trends and intra-basin sensitivity. *Global and Planetary Change*, 115:44 – 58, 2014. ISSN 0921-8181. doi: https://doi.org/10.1016/j.gloplacha.2014.01.011. URL http://www.sciencedirect.com/science/article/pii/S0921818114000289.

J. A. Cunge, M. Holly, F., and A. Verwey. *Practical Aspects of Computational River Hydraulics*. Pitam Publishing, 1980.

DassFlow. Dassflow: Data assimilation for free surface flows. Technical report, Mathematics Institute of Toulouse - INSA group - CNES - CNRS - ICUBE, 2018. URL http://www.math.univ-toulouse.fr/DassFlow.

G. Di Baldassarre, G. Schumann, and P. Bates. Near real time satellite imagery to support and verify timely flood modelling. *Hydrological Processes*, 23(5):799–803, 2009. doi: 10.1002/hyp.7229. URL https://onlinelibrary.wiley.com/doi/abs/10.1002/hyp.7229.

M. Durand, J. Neal, E. Rodríguez, K. M Andreadis, L. C. Smith, and Y. Yoon. Estimating reach-averaged discharge for the river severn from measurements of river water surface elevation and slope. *Journal of Hydrology*, 511:92–104, 2014.

M. Durand, CJ. Gleason, P-A. Garambois, D. Bjerklie, LC. Smith, H. Roux, E. Rodriguez, PD. Bates, TM. Pavelsky, J Monnier, et al. An intercomparison of remote sensing river discharge estimation algorithms from measurements of river height, width, and slope. *Water Resources Research*, 2016.

C. M. Emery, A. Paris, S. Biancamaria, A. Boone, S. Calmant, P.-A. Garambois, and J. S. da Silva. Large scale hydrological model river storage and discharge correction using satellite altimetry-based discharge product. *Hydrology and Earth System Sciences Discussions*, 2017:1–54, 2017. doi: 10.5194/hess-2017-516. URL `https://www.hydrol-earth-syst-sci-discuss.net/hess-2017-516/`.

Rob Ferguson. Flow resistance equations for gravel- and boulder-bed streams. *Water Resources Research*, 43(5), 2010. doi: 10.1029/2006WR005422. URL `https://agupubs.onlinelibrary.wiley.com/doi/abs/10.1029/2006WR005422`.

R. Frasson, R. Wei, M. Durand, J. Minear, A. Domeneghetti, G. Schumann, B. Williams, E. Rodriguez, C. Picamilh, C. Lion, T. Pavelsky, and P.-A. Garambois. Automated river reach definition strategies: Applications for the surface water and ocean topography mission. *Water Resources Research*, 53(10):8164–8186, 2017. ISSN 1944-7973. doi: 10.1002/2017WR020887. URL `http://dx.doi.org/10.1002/2017WR020887`.

P-A. Garambois and J. Monnier. Inference of effective river properties from remotely sensed observations of water surface. *Advances in Water Resources*, 79:103–120, 2015.

I. Gejadze and P.-O. Malaterre. Discharge estimation under uncertainty using variational methods with application to the full saint-venant hydraulic network model. *International Journal for Numerical Methods in Fluids*, 83(5): 405–430, 2017. ISSN 1097-0363. doi: 10.1002/fld.4273. URL `http://dx.doi.org/10.1002/fld.4273`. fld.4273.

I. Gejadze and J. Monnier. On a 2d zoom for the 1d shallow water model: Coupling and data assimilation. *Computer methods in applied mechanics and engineering*, 196(45):4628–4643, 2007. doi: https://doi.org/10.1016/j.cma.2007.05.026.

A. F. Gessese, M. Sellier, E. Van Houten, and G. Smart. Reconstruction of river bed topography from free surface data using a direct numerical approach in one-dimensional shallow water flow. *Inverse Problems*, 27(2):025001, 2011. URL `http://stacks.iop.org/0266-5611/27/i=2/a=025001`.

J. C. Gilbert and C. Lemaréchal. Some numerical experiments with variable-storage quasi-newton algorithms. *Mathematical programming*, 45(1-3):407–435, 1989.

C.J. Gleason and L. C. Smith. Toward global mapping of river discharge using satellite images and at-many-stations hydraulic geometry. *Proceedings of the National Academy of Sciences*, 111(13):4788–4791, 2014. ISSN 0027-8424. doi: 10.1073/pnas.1317606111. URL `http://www.pnas.org/content/111/13/4788`.

S. Haben, A. Lawless, and N. Nichols. Conditioning and preconditioning of the variational data assimilation problem. *Computers & Fluids*, 46(1):252–256, 2011a.

S. Haben, A. Lawless, and N. Nichols. Conditioning of incremental variational data assimilation, with application to the met office system. *Tellus A*, 63(4):782–792, 2011b.

L. Hascoët and V. Pascual. The Tapenade Automatic Differentiation tool: Principles, Model, and Specification. *ACM Transactions On Mathematical Software*, 39(3), 2013. URL `http://dx.doi.org/10.1145/2450153.2450158`.

M. Honnorat, X. Lai, F-X. le Dimet, and J. Monnier. Variational data assimilation for 2D fluvial hydraulics simulation. *CMWR XVI-Computational Methods for Water Ressources. Copenhagen, june 2006.*, 2006.

M. Honnorat, J. Monnier, and F.-X. Le Dimet. Lagrangian data assimilation for river hydraulics simulations. *Computing and Visualization in Science*, 12(5):235–246, 2009.

M. Honnorat, J. Monnier, N. Rivière, E. Huot, and F.-X. Le Dimet. Identification of equivalent topography in an open channel flow using lagrangian data assimilation. *Computing and visualization in science*, 13(3):111–119, 2010.

R. Hostache, X. Lai, J Monnier, and C. Puech. Assimilation of spatially distributed water levels into a shallow-water flood model. Part II: Use of a remote sensing image of Mosel River. *Journal of Hydrology*, 390:257–268, 2010. URL `http://www.sciencedirect.com/science/article/pii/S0022169410004166`. 3-4.

B. Kaltenbacher, A. Neubauer, and O. Scherzer. *Iterative regularization methods for nonlinear ill-posed problems*, volume 6. Walter de Gruyter, 2008.

X. Lai and J. Monnier. Assimilation of spatially distributed water levels into a shallow-water flood model. Part I: mathematical method and test case. *Journal of Hydrology*, 377:1–11, 2009. URL `http://www.sciencedirect.com/science/article/pii/S0022169409004508`. 1-2.

K. Larnier. *Modélisation thermohydraulique d'un tronçon de Garonne en lien avec l'habitat piscicole : Approches statistique et déterministe*. PhD thesis, Toulouse, 2010.

F.-X. Le Dimet and O. Talagrand. Variational algorithms for analysis and assimilation of meteorological observations: theoretical aspects. *Tellus A: Dynamic Meteorology and Oceanography*, 38(2):97–110, 1986.

L. B. Leopold and T. J Maddock. The hydraulic geometry of stream channels and some physiographic implications. *USGS Numbered Series*, 252:57pp, 1953. URL `https://pubs.er.usgs.gov/publication/pp252`. -.

J.-L. Lions. Optimal control of systems governed by partial differential equations problèmes aux limites. 1971.

A. Lorenc, S. Ballard, R. Bell, N. Ingleby, P. Andrews, D. Barker, J. Bray, A. Clayton, T. Dalby, D. Li, et al. The met. office global three-dimensional variational data assimilation scheme. *Quarterly Journal of the Royal Meteorological Society*, 126(570):2991–3012, 2000.

J. Marin and J. Monnier. Superposition of local zoom models and simultaneous calibration for 1d–2d shallow water flows. *Mathematics and Computers in Simulation*, 80(3):547–560, 2009.

J. Monnier. *Variational data assimilation: from optimal control to large scale data assimilation*. Open Online Course, INSA Toulouse, 2014.

J. Monnier, F. Couderc, D. Dartus, K. Larnier, R. Madec, and J-P. Vila. Inverse algorithms for 2D shallow water equations in presence of wet dry fronts. application to flood plain dynamics. *Advances in Water Resources*, 97: 11–24, 2016.

S. Munier, A. Polebistki, C. Brown, G. Belaud, and D. P. Lettenmaier. Swot data assimilation for operational reservoir management on the upper niger river basin. *Water Resources Research*, 51(1):554–575, 2015. ISSN 1944-7973. doi: 10.1002/2014WR016157. URL `http://dx.doi.org/10.1002/2014WR016157`.

I. Navon. Practical and theoretical aspects of adjoint parameter estimation and identifiability in meteorology and oceanography. *Dynamics of Atmospheres and Oceans*, 27(1):55 – 79, 1998. ISSN 0377-0265. doi: https://doi.org/10.1016/S0377-0265(97)00032-8. URL `http://www.sciencedirect.com/science/article/pii/S0377026597000328`.

C. Ottle and J.-M. Mahfouf. Data assimilation of satellite observations. In N. Baghdadi and M. Zribi, editors, *Microwave Remote Sensing of Land Surface*, pages 357–382. Elsevier, 2016. ISBN 978-1-78548-159-8. doi: https://doi.org/10.1016/B978-1-78548-159-8.50008-6. URL `https://www.sciencedirect.com/science/article/pii/B9781785481598500086`.

H Oubanas, I Gejadze, P-O Malaterre, and F Mercier. River discharge estimation from synthetic swot-type observations using variational data assimilation and the full saint-venant hydraulic model. *Journal of Hydrology*, 559:638–647, 2018.

D. Paiva, W. Collischonn, M.-P. Bonnet, F. Frappart, S. Calmant, and C. Bulhques Mendes. Large-scale hydrologic and hydrodynamic modeling of the amazon river basin. *Water Resources Research*, 49(3):1226–1243. doi: 10.1002/wrcr.20067. URL `https://agupubs.onlinelibrary.wiley.com/doi/abs/10.1002/wrcr.20067`.

R. Paiva, W. Collischonn, and C. Tucci. Large scale hydrologic and hydrodynamic modeling using limited data and a gis based approach. *Journal of Hydrology*, 406(3-4):170–181, 2011.

V.G. Panchang and J.J. O'Brien. On the determination of hydraulic model parameters using the adjoint state formulation. *Modeling marine system*, 1:5–18, 1989.

S. Ricci, A. Piacentini, O. Thual, E. Le Pape, and G. Jonville. Correction of upstream flow and hydraulic state with data assimilation in the context of flood forecasting. *Hydrol. Earth Syst. Sci.*, 15:3555–3575, 2011. URL `http://www.hydrol-earth-syst-sci.net/15/3555/2011/ http://www.hydrol-earth-syst-sci.net/15/3555/2011/hess-15-3555-2011.pdf`. 11.

E. Rodríguez. SWOT Science requirements document. JPL document, JPL, 2012.

W. Rogers. Central valley floodplain evaluation and delineation. Document, 2014.

H. Roux and D. Dartus. Use of parameter optimization to estimate a flood wave: Potential applications to remote sensing of rivers. *J. of Hydrology*, 328:258–266, 2006.

B.F. Sanders and N.D. Katopodes. Control of canal flow by adjoint sensitivity method. *Journal of irrigation and drainage engineering*, 125(5):287–297, 1999.

Y. Sasaki. *Some basic formalisms in numerical variational analysis.* Citeseer, 1970.

Kutalmis Saylam, Rebecca A. Brown, and John R. Hupp. Assessment of depth and turbidity with airborne lidar bathymetry and multiband satellite imagery in shallow water bodies of the alaskan north slope. *International Journal of Applied Earth Observation and Geoinformation*, 58:191 – 200, 2017. ISSN 0303-2434. doi: https://doi.org/10.1016/j.jag.2017.02.012. URL http://www.sciencedirect.com/science/article/pii/S0303243417300387.

J. Schellekens, E. Dutra, A. Martínez-de la Torre, G. Balsamo, A. van Dijk, F. Sperna Weiland, M. Minvielle, J.-C. Calvet, B. Decharme, S. Eisner, G. Fink, M. Flörke, S. Peßenteiner, R. van Beek, J. Polcher, H. Beck, R. Orth, B. Calton, S. Burke, W. Dorigo, and G. P. Weedon. A global water resources ensemble of hydrological models: the earth2observe tier-1 dataset. *Earth System Science Data*, 9(2):389–413, 2017. doi: 10.5194/essd-9-389-2017. URL https://www.earth-syst-sci-data.net/9/389/2017/.

A. Tarantola. *Inverse problem theory and methods for model parameter estimation*, volume 89. SIAM, 2005.

D. Wisser, B. Fekete, C Vörösmarty, and A Schumann. Reconstructing 20th century global hydrography: a contribution to the global terrestrial network-hydrology (gtn-h). *Hydrology and Earth System Sciences*, 14(1):1, 2010.

Y. Yoon, M. Durand, C.J. Merry, E.A. Clark, K.M. Andreadis, and Alsdorf D.E. Estimating river bathymetry from data assimilation of synthetic swot measurements. *Journal of Hydrology*, 464 - 465 (0):363 – 375, 2012. ISSN 0022-1694. doi: http://dx.doi.org/10.1016/j.jhydrol.2012.07.028. URL http://www.sciencedirect.com/science/article/pii/S0022169412006294.

Y. Yoon, P-A. Garambois, R. Paiva, M. Durand, H. Roux, and E. Beighley. Improved error estimates of a discharge algorithm for remotely sensed river measurements: Test cases on Sacramento and Garonne Rivers. *Water Resources Research*, 52(1):278–294, 2016.